9-20-2001

The Discovery of Cepheids and a New Distance to NGC 2841 Using the Hubble Space Telescope

L. M. Macri
Harvard-Smithsonian Center for Astrophysics

P. B. Stetson
National Research Council of Canada

G. D. Bothun
University of Oregon

W. L. Freedman
Observatories of the Carnegie Institute of Washington

P. M. Garnavich
University of Notre Dame

See next page for additional authors

Recommended Citation
L. M. Macri et al 2001 ApJ 559 243 https://doi.org/10.1086/322395

To appear in the September 20, 2001 issue of the Astrophysical Journal

THE DISCOVERY OF CEPHEIDS AND A NEW DISTANCE TO NGC 2841 USING THE HUBBLE SPACE TELESCOPE†

L.M. Macri[1], P.B. Stetson[2], G.D. Bothun[3], W.L. Freedman[4], P.M. Garnavich[5], S. Jha[1], B.F. Madore[4,6] & M.W. Richmond[7]

ABSTRACT

We report on the discovery of Cepheids in the spiral galaxy NGC 2841, based on observations made with the Wide Field and Planetary Camera 2 on board the *Hubble Space Telescope*. NGC 2841 was observed over 12 epochs using the F555W filter, and over 5 epochs using the F814W filter. Photometry was performed using the DAOPHOT/ALLFRAME package.

We discovered a total of 29 variables, including 18 high-quality Cepheids with periods ranging from 15 to 40 days. Period-luminosity relations in the V and I bands, based on the high-quality Cepheids, yield a reddening-corrected distance modulus of 30.74 ± 0.23 mag, which corresponds to a distance of 14.1 ± 1.5 Mpc. Our distance is based on an assumed LMC distance modulus of $\mu_0 = 18.50 \pm 0.10$ mag ($D = 50 \pm 2.5$ kpc) and a metallicity dependence of the Cepheid P-L relation of $\gamma_{VI} = -0.2 \pm 0.2$ mag/dex.

Subject headings: Cepheids — distance scale — galaxies: individual (NGC 2841)

1. INTRODUCTION

This paper presents the discovery of 26 Cepheids and a distance determination to NGC 2841. NGC 2841 is an isolated, flocculent spiral galaxy, classified as Sb(r): I (de Vaucouleurs et al. 1991) or Sb I (Sandage & Tammann 1981), and located at $\alpha = 9^{\rm h}\ 22^{\rm m}\ 03^{\rm s}$, $\delta = +50^\circ\ 58'\ 36''$ (J2000.0). It exhibits a heliocentric redshift of +683 km/s, and has a major axis diameter of 8.′3. Tully (1988) places it in the northwestern-most association of the Leo Spur (Group 15+10).

The inclination angle of NGC 2841 is 64° (de Vaucouleurs et al. 1991), making it a suitable calibrator of the Tully-Fisher relation. Furthermore, the large observed 21-cm line-width of NGC 2841 (614 ± 4 km/s, Rothberg et al. 2000) significantly extends the range in rotation velocity over which the Tully-Fisher relation has been calibrated using Cepheid distances. This topic will be covered by Bothun et al. (2001), which will also address the implications of the NGC 2841 Cepheid distance regarding the predictions from the MOND (MOdified Newtonian Dynamics) theory.

NGC 2841 has been the host of four supernovae in the last century: SN 1912A, SN 1957A, SN 1972R and SN 1999by. The last one is a well-observed type Ia SN which has been classified as a fast decliner (hence subluminous). Thus, it is of special importance for the calibration of the type Ia SNe distance indicator. This topic will be addressed by Garnavich et al. (2001).

§2 describes the observations and preliminary reductions of the images. §3 contains the details of photometry and calibration of the instrumental magnitudes. §4 presents the sample of variables and their properties. §5 describes the fiducial Cepheid Period-Luminosity relations used in our analysis, derives a distance modulus, and lists the sources of uncertainty. §6 discusses some implications of our distance measurement, and §7 presents our conclusions.

2. OBSERVATIONS AND REDUCTIONS

NGC 2841 was observed by the Wide Field and Planetary Camera 2 (WFPC2) (Biretta et al. 2000) on board HST on twelve epochs between 2000 February 29 and April 19. The observations were performed using the F555W (approximately Johnson V) and the F814W (approximately Kron-Cousins I) filters. All twelve epochs contained a pair of CR-split images in the F555W band, while five epochs contained an additional pair of CR-split images in the F814W. Each individual image had an exposure time of 1100s. All observations were made with the telescope guiding in fine lock with a stability of approximately 3 mas. The gain and readout noise were 7 e^-/DN and 7 e^-, respectively. The CCD was operated at a temperature of –88° C for all observations. A log of the observations is presented in Table 1. The sampling strategy followed in these observations was similar to the one employed by the *HST* Key Project on the Extragalactic Distance Scale (Freedman et al. 2001), It followed a power-law distribution in time, which provides an optimum sampling of the light curves of Cepheids in the period range between 10 and 50 days.

[1] Harvard-Smithsonian Center for Astrophysics, 60 Garden St., Cambridge, MA 02138, USA. lmacri@cfa.harvard.edu

[2] Dominion Astrophysical Observatory, Herzberg Institute of Astrophysics, National Research Council of Canada, 5071 West Saanich Road, Victoria, BC V8X 4M6, Canada.

[3] Department of Physics, University of Oregon, 1371 E 13th Ave., Eugene, OR 97403, USA.

[4] Observatories of the Carnegie Institution of Washington, 813 Santa Barbara St., Pasadena, CA 91101, USA.

[5] Physics Department, 225 Nieuwland Science Hall, University of Notre Dame, Notre Dame, IN 46556, USA.

[6] Infrared Analysis and Processing Center, California Institute of Technology, 770 South Wilson Avenue, Pasadena CA 91125, USA.

[7] Physics Department, Rochester Institute of Technology, 1 Lomb Memorial Dr., Rochester, NY 14623

† Based on observations with the NASA/ESA *Hubble Space Telescope*, obtained at the Space Telescope Science Institute, operated by AURA, Inc. under NASA contract No. NAS5-26555.

The images were calibrated using the pipeline processing at the Space Telescope Institute (STScI). The full reduction procedure (Holtzman et al. 1995a) consisted of: a correction for A/D conversion errors, the subtraction of a bias level for each chip, the subtraction of a superbias frame, the subtraction of a dark frame, a correction for shutter shading, and a division by a flat field. Furthermore, the images were corrected for vignetting and geometrical distortions in the WFPC2 optics (the latter correction was done using files kindly provided by J. Holtzman). Lastly, the images were multiplied by four and converted to two-byte integers, to reduce disk usage and allow image compression. This conversion led to an effective readout noise of 4 DN and a gain of 1.75e$^-$/DN.

Figure 1 displays a ground-based image of NGC 2841, obtained at the Whipple Observatory 1.2-m telescope, with a super-imposed mosaic of the WFPC2 field of view. The mosaic is shown in greater detail in Figure 2.

3. PHOTOMETRY AND CALIBRATION

Photometry of NGC 2841 was performed using the DAOPHOT/ALLFRAME package. Stetson (1994, 1998) contain comprehensive overviews of the package and the reduction strategy, which we briefly summarize here.

As in the case of previous ALLFRAME reductions of WFPC2 data, we used external point-spread functions (PSFs), determined by P.B.S. for each chip and filter combination from high S/N, uncrowded observations of Galactic globular cluster fields. These external PSFs take into account the variation in the PSF across the field of view of each WFPC2 chip.

The photometric reduction started with a preliminary detection of sources in each individual image. DAOMATCH and DAOMASTER were used to derive offsets and rotations between frames, relative to the first F555W frame. In the case of these observations, the shifts were < 1 pixel for 31 frames, and ~ 2 pixels for the other two. Once the transformations were established, MONTAGE was used to create a medianed image, free of cosmic rays and chip defects. The FIND routine in DAOPHOT was used to detect the sources present in that image, and their positions were refined by running ALLSTAR. The resulting list of objects was used by ALLFRAME to perform the photometry of each object in every frame.

The conversion from PSF to standard (Holtzman et al. 1995b) $0.5''$-radius aperture magnitudes involved the determination of growth curves. First, we selected bright and isolated stars (hereafter, "secondary standards") that were located in areas with low and slowly-varying backgrounds. Next, all other objects were removed from the frames and aperture photometry was carried out at a variety of radii. DAOGROW (Stetson 1990) was used to derive growth curves and to obtain $0.5''$-radius aperture magnitudes for the secondary standards in each frame. Lastly, we used COLLECT to calculate the "aperture correction" coefficient for each frame from the difference between PSF and aperture magnitudes of the secondary standards.

The conversion from $F555W$ and $F814W$ magnitudes to Johnson V and Kron-Cousins I bandpasses followed the precepts of Holtzman et al. (1995b):

$$V = F555W - 0.052[\pm0.007]\ (V-I) + 0.027[\pm0.002]\ (V-I)^2 + Z_{i,F555W} \quad (1)$$

$$I = F814W - 0.062[\pm0.009]\ (V-I) + 0.025[\pm0.002]\ (V-I)^2 + Z_{i,F814W} \quad (2)$$

where $F555W$ and $F814W$ equal $-2.5\log(\mathrm{DN\ s^{-1}})$ and the color terms come from Table 7 of Holtzman et al. (1995b). The zeropoint terms (Z_i), which are listed in Table 2, were determined by P.B.S. and reflect evolution in the understanding of the WFPC2 calibration since the publication of Stetson (1998) (cf. Table 5 of that paper). For those epochs without F814W data, the transformation of the $F555W$ magnitudes into the standard V bandpass was carried out using the mean $V-I$ color of each object.

Additionally, the magnitudes of each object were corrected for the effects of charge transfer inefficiency following the prescription of Stetson (1998). In order to facilitate the comparison of our magnitude system with future studies, we list in Table 3 the mean V and I magnitudes for the secondary standards present in each chip.

4. THE CEPHEIDS FOUND IN NGC 2841

The initial search for variables was carried out using TRIAL, a program that calculated the value of the J statistic for each star, based on the V-band data. The J statistic is a robust index of variability developed by Stetson (1996), and it is designed so that objects with constant magnitudes yield values near zero. The mean value and *r.m.s.* deviation of this index for all stars present in our database was 0.01 ± 0.29. We flagged 79 objects with $J > 0.8$ as possible variables, and extracted their individual light curves from the photometry database for further analysis using a suite of programs developed by the DIRECT team (Kaluzny et al. 1998).

We calculated periods for the candidate variables using a modified version of the Lafler-Kinman technique (Stetson 1996); we restricted the range of possible periods to the range between 10 and 50 days. Next, template Cepheid light curves (derived by Stetson 1996) were simultaneously fitted to the phased V- and I-band photometry of each candidate. The use of templates allows a robust classification of a candidate variable as a Cepheid, refines the period of the variable, and yields reliable mean magnitudes through numerical integration of the best-fit template. If the candidate object was classified as a Cepheid, an iterative 3σ rejection algorithm was applied to the data to reject anomalous photometric measurements, most of them associated with cosmic-ray hits, and the light curve was analyzed again. About 5% of the individual data points were rejected in this manner.

The automated classification software rejected 50 candidates and classified 26 objects as Cepheids. An additional 3 objects are clearly variables, and most likely Cepheids, but their periods are longer that our observing window and we cannot obtain accurate values for their mean magnitudes. Table 4 lists the following properties of the 29 variables which passed the analysis: identification number (C01-C26 in order of descending period, for the Cepheids, and V01-V03 in order of increasing R.A., for the other variables); chip where the object is located; (x, y) coordinates

(based on the coordinate system of the first V band image); J2000.0 coordinates; best-fit period and uncertainty (Cepheids only); V and I mean magnitudes, derived from the best-fit template light curves; and a selection flag (see §5.2 for details).

Figure 3 contains chip-wide images of each of the WFPC2 CCDs, indicating the locations of the variables. Finding charts for each of the stars are displayed in Figure 4; the charts encompass a 50 by 50 pixel area around each variable (i.e., $2''.15 \times 2''.15$ for the PC and $5'' \times 5''$ for the WF). The individual V and I band photometric measurements are listed in Tables 5 and 6, respectively, and shown as phase-magnitude plots (for the Cepheids) and as time series (for the other variables) in Figure 5. That Figure also shows the V and I best-fit template light curves for each Cepheid, which were used to determine their mean magnitudes.

Figure 6 shows a color-magnitude diagram of the ~ 9000 stars detected in our images. As expected, the Cepheids occupy a region of the diagram that is consistent with the location of the instability strip. Figure 7 shows the observed differential luminosity functions for the V and I data, which indicate that our completeness limits are V$\sim$ 26.5 mag and I$\sim$ 25.5 mag. Additionally, the I band luminosity function does not exhibit the signature associated with the Tip of the Red Giant Branch (c.f. Figure 2 of Sakai et al. 2000), yielding a lower limit for the distance to NGC 2841 of ~ 29.5 mag or ~ 8 Mpc.

5. PERIOD-LUMINOSITY RELATIONS AND DISTANCE MODULI

5.1. *Methodology*

The method used to derive V- and I-band apparent distance moduli is the same one that was used by the *HST* Key Project on the Extragalactic Distance Scale, which is described in detail by Freedman et al. (2001). It relies on fiducial Period-Luminosity relations of LMC Cepheids, corrected for reddening and scaled based on an assumed true distance modulus of $\mu_{0,\rm LMC} = 18.50 \pm 0.10$ mag. The P-L relations used are those from (Udalski et al. 1999), based on a sample of ~ 650 OGLE Cepheids with periods ranging from 2.5 to 28 days:

$$M_V = -2.760(\pm 0.03)\,[\log P - 1] - 4.218(\pm 0.02), \quad (3)$$

$$M_I = -2.962(\pm 0.02)\,[\log P - 1] - 4.904(\pm 0.04). \quad (4)$$

These relations can be combined to obtain an equation for the reddening-corrected distance modulus of a Cepheid (Freedman et al. 2001):

$$\mu_0 = W + 3.255(\pm 0.01)\,[\log \mathrm{P} - 1] + 5.899(\pm 0.01), \quad (5)$$

where $W = V - 2.45(V-I)$ is the reddening-free Wesenheit magnitude (Madore 1982).

5.2. *Distance moduli*

Before determining distance moduli from Equations 3-5, we must impose a cut in period at the short end to avoid an incompleteness bias (see Appendix A of Freedman et al. 2001). The completeness limits determined at the end of §4 imply that this cut must be applied around $P = 20$ d, resulting in the rejection of Cepheids C01-C05. We also rejected Cepheids C07-C09 due to their rather poor quality I band light curves. Thus, the final sample of Cepheids used for distance determination consists of 18 variables, identified with an asterisk in the last column of Table 4.

Figures 8 and 9 show the V and I band P-L relations of the final sample of Cepheids. By fitting the P-L relations described in Equations (3) and (4), we obtain apparent V and I band distance moduli of $\mu_V = 31.23 \pm 0.08$ mag and $\mu_I = 30.96 \pm 0.06$ mag (internal errors only), and a mean color excess of $E(V-I) = 0.27 \pm 0.03$ mag. The application of Equation (5) results in an extinction-corrected distance modulus of $\mu_0 = 30.58 \pm 0.06$ mag (internal errors only).

5.3. *Metallicity correction*

The measured value of μ_0 must be corrected for the metallicity dependence of the Cepheid P-L relation, using the following equation:

$$\delta\mu_Z = \gamma_{VI}\,\big([O/H]_{N2841} - [O/H]_{LMC}\big), \quad (6)$$

where γ_{VI} is the metallicity dependence index for the V and I filters, and $[O/H]_{gal} = \log(O/H)_{gal}/\log(O/H)_{\odot}$. We adopt $\gamma_{VI} = 0.2 \pm 0.2$ mag/dex (Freedman et al. 2001), which represents the range of measurements found in the literature (Kochanek 1997; Sasselov et al. 1997; Kennicutt et al. 1998). The adopted $[O/H]$ value for the LMC is -0.4 dex (Kennicutt et al. 1998).

The $[O/H]$ value for our field in NGC 2841 can be calculated using $([O\,II]\lambda\lambda 3727)/H\beta$ and $([O\,III]\lambda\lambda 4959, 5007)/H\beta$ line flux ratios listed in Table 3 of Bresolin et al. (1999) for four HII regions located at galactocentric radii similar to those spanned by our Cepheids. The sum of these two line flux ratios (known as R_{23}) can be turned into a value of $[O/H]$ by using the appropriate Equation from Zaritsky et al. (1994). We find $[O/H]_{N2841} = 0.4 \pm 0.15$ dex, which reflects the scatter in the abundances of the four HII regions (± 0.07) and the uncertainty in the calibration of the metallicity-R_{23} relation for high abundances.

In conclusion, Equation (6) results in an overall correction of $\delta\mu_Z = +0.16 \pm 0.15$ mag to our distance modulus, making it $\mu_{0,Z} = 30.74 \pm 0.23$ mag. This uncertainty includes several sources of error, which we list in the following sub-section.

5.4. *Error Budget*

The error budget for our distance determination is listed in Table 7, and explained in greater detail here. The internal error due to the dispersion in individual values of μ_0 is a small contribution to the total error, which is heavily dominated by external sources of error. These are, in decreasing order of importance: the metallicity dependence of the Cepheid P-L relation, the distance to the LMC, the absolute calibration of WFPC2, contamination of the Cepheid magnitudes due to unresolved blends, and the uncertainty in the reddening law of NGC 2841.

i. Metallicity correction: As stated in §5.3, the uncertainty in the adopted value of the metallicity correction index γ_{VI} is ± 0.2 mag/dex, and the uncertainty in the difference in abundances between the LMC and NGC 2841 is ± 0.15 dex. The combination of these two uncertainties results in a contribution to the error budget of ± 0.15 mag.

ii. LMC Distance: The uncertainty in the distance to the LMC has been recently summarized by Freedman et al. (2001). We have adopted $\mu_0(\mathrm{LMC}) = 18.50 \pm 0.10$ mag in order to maintain consistency with the Cepheid distances presented in that paper. However, different distance indicators yield widely different (and non-overlapping) estimates of the LMC distance modulus, ranging from 18.3 to 18.65 mag (see Table 13 of Freedman et al. 2001).
iii. Blending: An additional source of uncertainty is the possible contamination of our Cepheid magnitudes by nearby stars, physically unrelated to the variables, but located at distances smaller than the resolution provided by the telescope and detector. Mochejska et al. (2001) have studied this contamination by comparing ground-based and HST images of long-period ($P > 10d$) Cepheids in M33. They conclude that the median value of this effect on HST data for galaxies at 10–15 Mpc is $\sim 7\%$ in V and $\sim 12\%$ in I. If these numbers were to apply to our Cepheids, our W magnitudes would be biased by 5%, or 0.1 mag. We take this value to represent a 1σ uncertainty due to the possible effects of blending.
iv. WFPC2 calibration: Freedman et al. (2001) have estimated the size of the uncertainty related to the absolute photometric calibration of WFPC2 to be ± 0.07 mag; this includes the uncertainties in the characterization of the zeropoints, the color transformations, the camera gain ratios, and the effects of CTE.
v. Reddening law: The reddening-free Wesenheit magnitudes used in Equation (5) were calculated using an assumed value of total-to-selective extinction $R \equiv A_V/E(B-V) = 3.1 \equiv A_V/E(V-I) = 2.45$. If the interstellar medium of NGC 2841 were to follow a different extinction law than the ISM of the Milky Way, the adoption of the standard value of R would introduce an additional systematic error to our distance estimate. This issue was addressed in a recent study by Macri et al. (2001), who obtained NICMOS H band photometry of extragalactic Cepheids in a dozen galaxies. They found that the extinction corrections determined from either V and I data or from V and H data, using the standard extinction law, are consistent with each other. Thus, the assumption of a standard reddening law is a valid one, and does not introduce a significant source of error.

The aforementioned sources of error (i-iv) can be combined in quadrature to arrive at a total external uncertainty in our metallicity-corrected true distance modulus of $+0.22, -0.19$ mag. The addition of the internal error term (± 0.06 mag) increases the total uncertainty to $+0.23, -0.20$ mag, which we simplify as ± 0.23 mag.

6. DISCUSSION

NGC 2841 is one of eight galaxies with Cepheid distances associated with the Leo Cloud & Spur, out of a total of 65 members listed in Tully (1988). Table 8 lists some properties of those eight galaxies. All distances (except for the one derived in this paper) are from Freedman et al. (2001). The mean velocity and dispersion of the previously observed galaxies is 727 ± 96 km/s, while the average distance (excluding the nearby NGC 3621) is 11.5 ± 0.6 Mpc. The small velocity dispersion for this relatively spread out structure is somewhat surprising, but consistent with bulk motion of the Leo Cloud. Kinematically, at a redshift of 638 ± 3 km/s, NGC 2841 is clearly a member of the Leo Spur, and our derived distance of 14.1 ± 1.5 Mpc places it on the far side of this structure.

Figure 10 shows the BVRI surface brightness profiles of NGC 2841 calculated from CCD images obtained at the Fred L. Whipple Observatory 1.2-m telescope. The procedure we followed to obtain these profiles is identical to the one described in Macri et al. (2000). We find a $B = 25$ mag/$\Box''$ isophotal radius of $\sim 280''$, which corresponds to a linear isophotal radius of ~ 40 kpc, given the distance of 14.1 ± 1.5 Mpc derived in the previous section. Thus, NGC 2841 is an impressively large disk galaxy, about twice the size of M31, a galaxy which shares many of its properties. Furthermore, the values of extinction-corrected effective radius, $r_e^i \sim 6$ kpc, and extinction-corrected effective surface brightness, $\langle\mu\rangle_e^i \sim 19.5$ I mag/$\Box''$, place NGC 2841 in a relatively unique position in the surface brightness – radius plane (see Figure 2 of de Jong & Lacey 2000).

7. CONCLUSIONS

We have discovered a total of 26 Cepheids and 3 other variables in the Sb spiral galaxy NGC 2841, a member of the Leo Spur. We have applied fiducial OGLE LMC V- and I-band Cepheid Period-Luminosity relations to a subsample of 18 Cepheids. We adopted an LMC distance of $\mu_0(\mathrm{LMC}) = 18.50 \pm 0.10$ mag, and a metallicity dependence of $\gamma_{VI} = 0.2 \pm 0.2$ mag/dex. Based on these assumptions, we obtain a distance modulus of 30.74 ± 0.23 mag, corresponding to a distance of 14.1 ± 1.5 Mpc. Our distance estimate is consistent with an association of this galaxy to the Leo Spur. The mean reddening of the Cepheid sample is $E(V-I) = 0.27 \pm 0.03$ mag.

A companion paper by Bothun et al. (2001) will address the impact of the Cepheid distance to NGC 2841 on the absolute calibration of the Tully-Fisher relation, as well as the implication of our distance for the MOND theory. A second companion paper by Garnavich et al. (2001) will combine our Cepheid distance with observations of SN 1999by to further the absolute calibration of the type Ia SNe distance indicator.

We would like to thank the referee, John Graham, for his helpful comments, and the STScI and NASA support staff that have made these observations possible. This work has made use of the NASA/IPAC Extragalactic Database (NED), which is operated by the Jet Propulsion Laboratory, Caltech, under contract with the National Aeronautics and Space Administration.

REFERENCES

Biretta, J.A., et al. 2000, *Wide Field and Planetary Camera 2 Instrument Handbook, Version 5.0* (Baltimore: STScI)
Bothun, G.D., et al. 2001, ApJ, in preparation
Bresolin, F., et al. 1999, ApJ, 510, 104
de Jong, R.S. & Lacey, C. 2000, ApJ, 545, 781
de Vaucouleurs, G., et al. 1991, *Third Reference Catalogue of Bright Galaxies* (Berlin: Springer-Verlag)
Freedman, W.L., et al. 2001, ApJ, 553, 47
Garnavich, P.M., et al. 2001, ApJ, submitted
Hill, R.J., et al. 1998, ApJ, 496, 648
Holtzman, J.A., et al. 1995a, PASP, 107, 156

Holtzman, J.A., et al. 1995b, PASP, 107, 1065
Kaluzny, J., et al. 1998, AJ, 115, 1016
Kennicutt, R.C., et al. 1998, ApJ, 498, 181
Kochanek, C.S. 1997, ApJ, 491, 13
Madore, B.F. 1982, ApJ, 253, 575
Macri, L.M., et al. 2000, ApJS, 128, 461
Macri, L.M., et al. 2001, ApJ, 548, xxx
Mochejska, B.J., et al. 2001, AJ, in preparation
Rothberg, B., et al. 2000, ApJ, 533, 781
Sakai, S., et al. 2000, AJ, 119, 1197
Sandage, A. & Tammann, G. 1981, *Revised Shapley-Ames Catalog of Bright Galaxies* (Washington: Carnegie)
Sasselov, D.D., et al. 1997, A&A, 324, 471
Stetson, P.B. 1990, PASP, 102, 932
Stetson, P.B. 1994, PASP, 106, 250
Stetson, P.B. 1996, PASP, 108, 851
Stetson, P.B. 1998, PASP, 110, 1448
Tully, R.B. & Fisher, J.R. 1987, *Nearby Galaxies Atlas* (Cambridge; New York: Cambridge University Press)
Tully, R.B. 1988, *Nearby Galaxies Catalog* (Cambridge; New York: Cambridge University Press)
Udalski, A., et al. 1999, Ac.A., 49, 201
Zaritsky, D., et al. 1994, ApJ, 420, 87

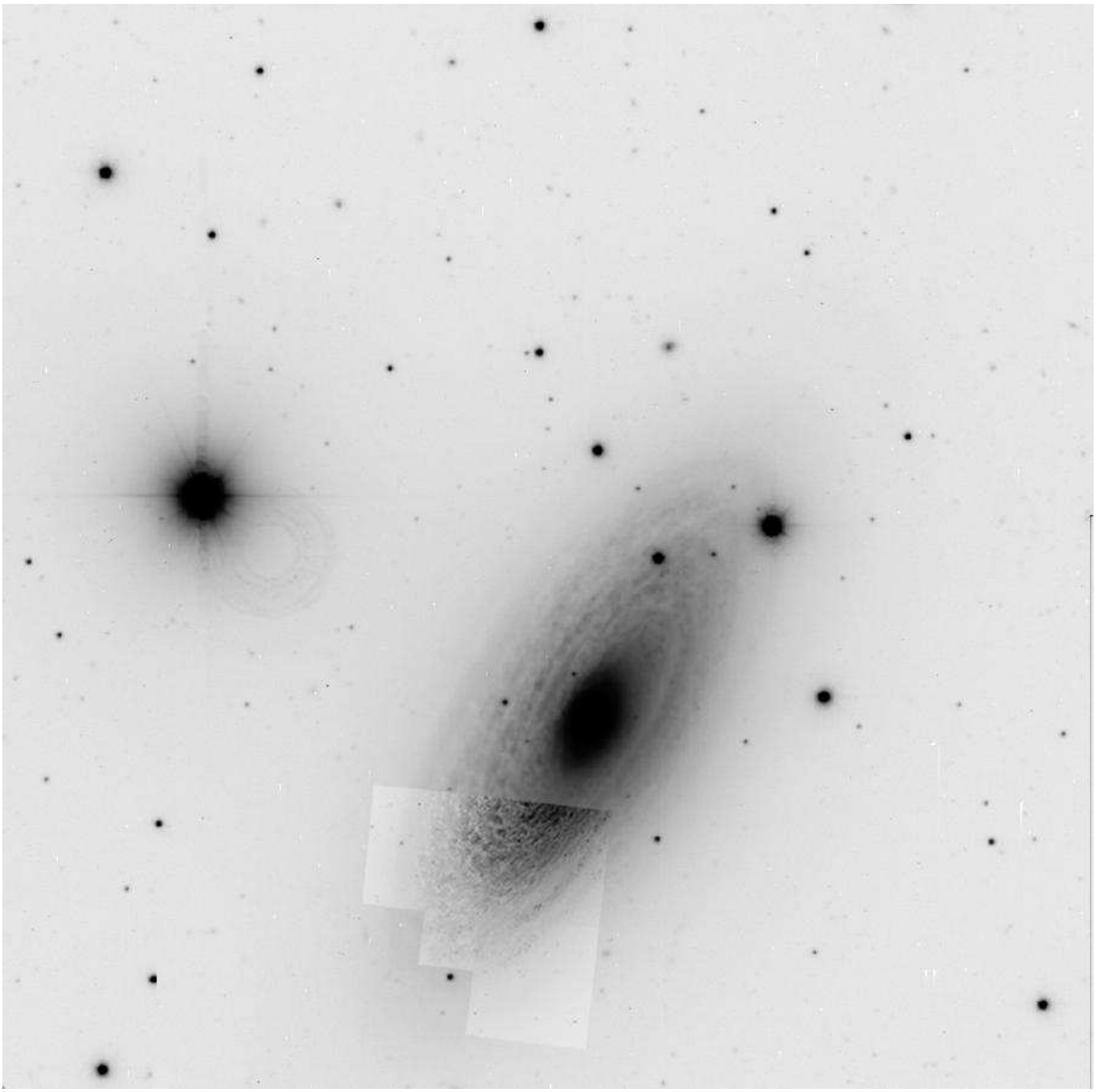

FIG. 1.— Ground-based image of NGC 2841, obtained at the FLWO 1.2-m telescope, with a super-imposed mosaic of the WFPC2 field of view (see Figure 2). North is up and east is to the left.

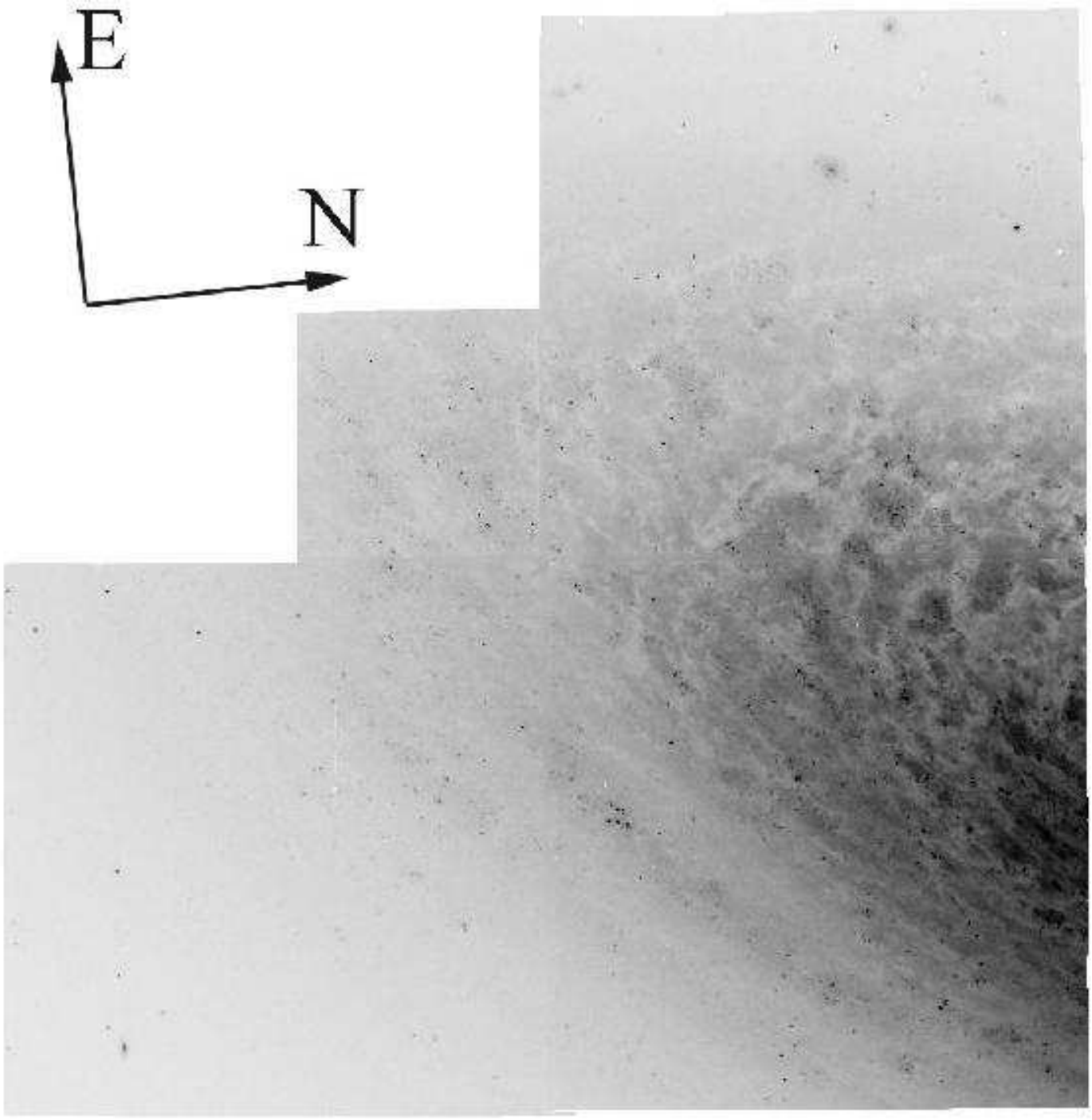

FIG. 2.— Mosaic of the WFPC2 field of view of NGC 2841. Individual images of each chip, showing the location of the variables, can be found in Figures 3a-d.

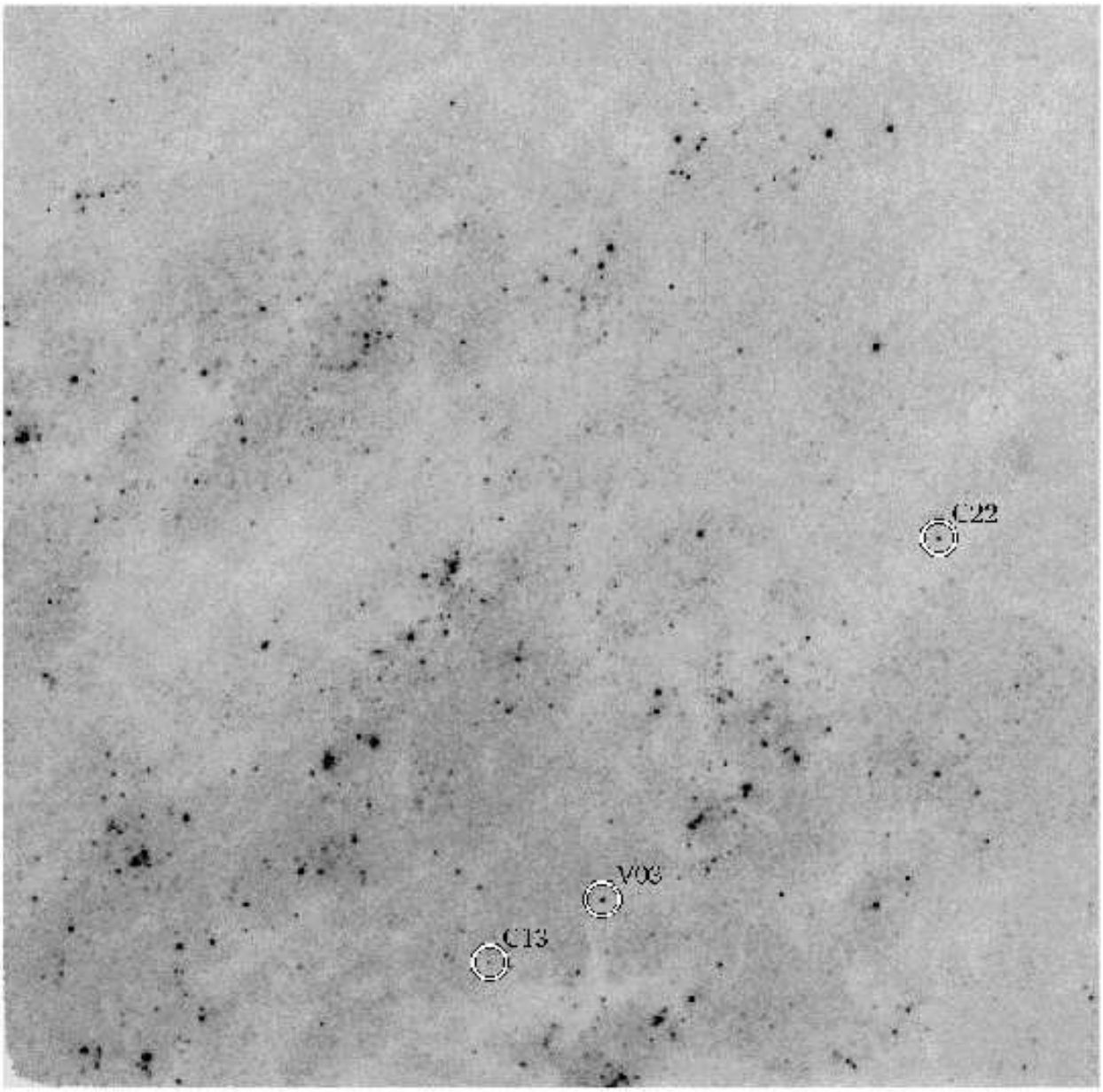

FIG. 3.— (a) Medianed images of the four WFPC2 chips. The circles indicate the position of each of the variables, labeled as in Table 3. Each of the images is oriented such that the bottom left corner has the pixel coordinates (0,0) in each image.

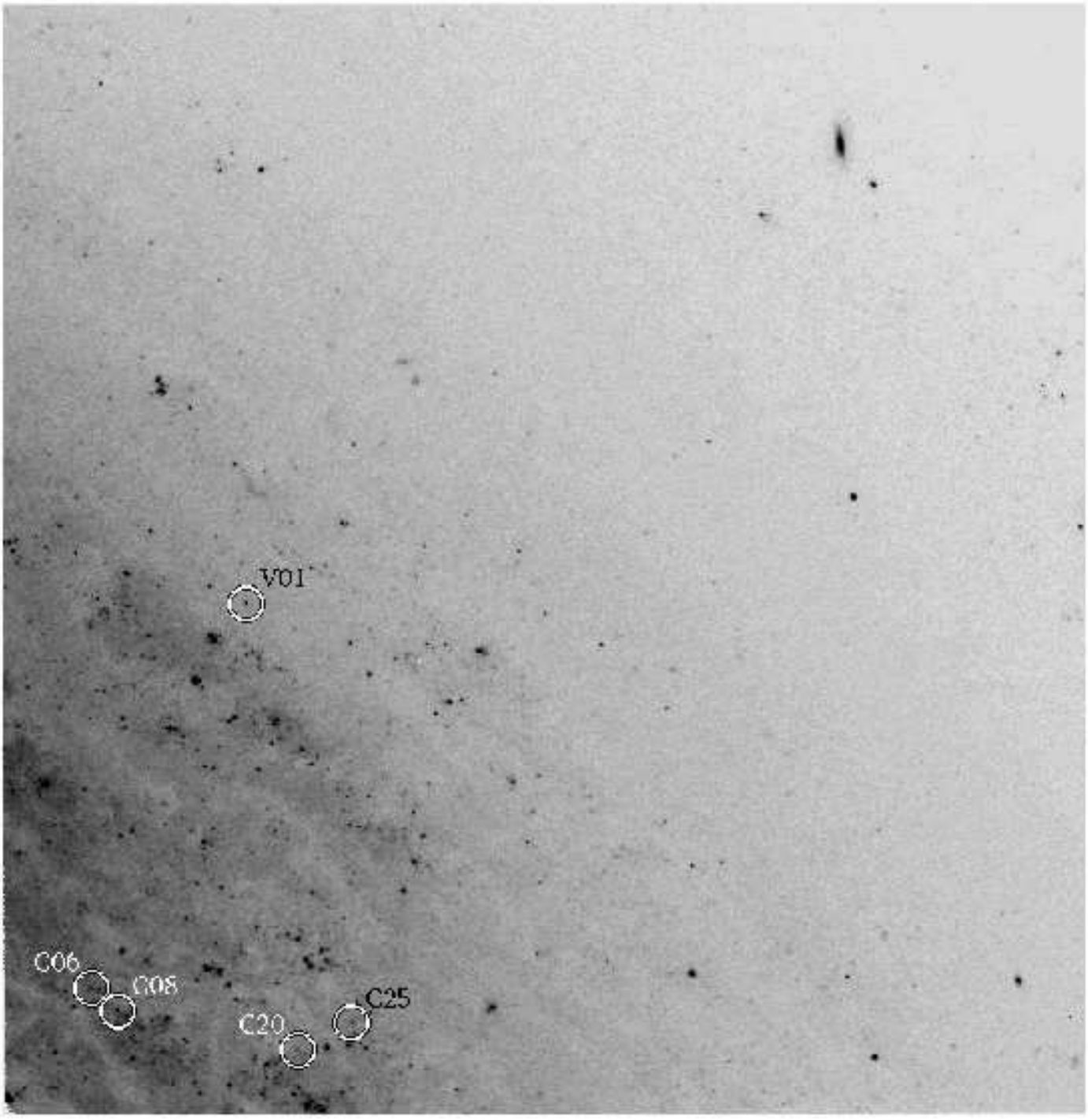

FIG. 3.— (b) continued.

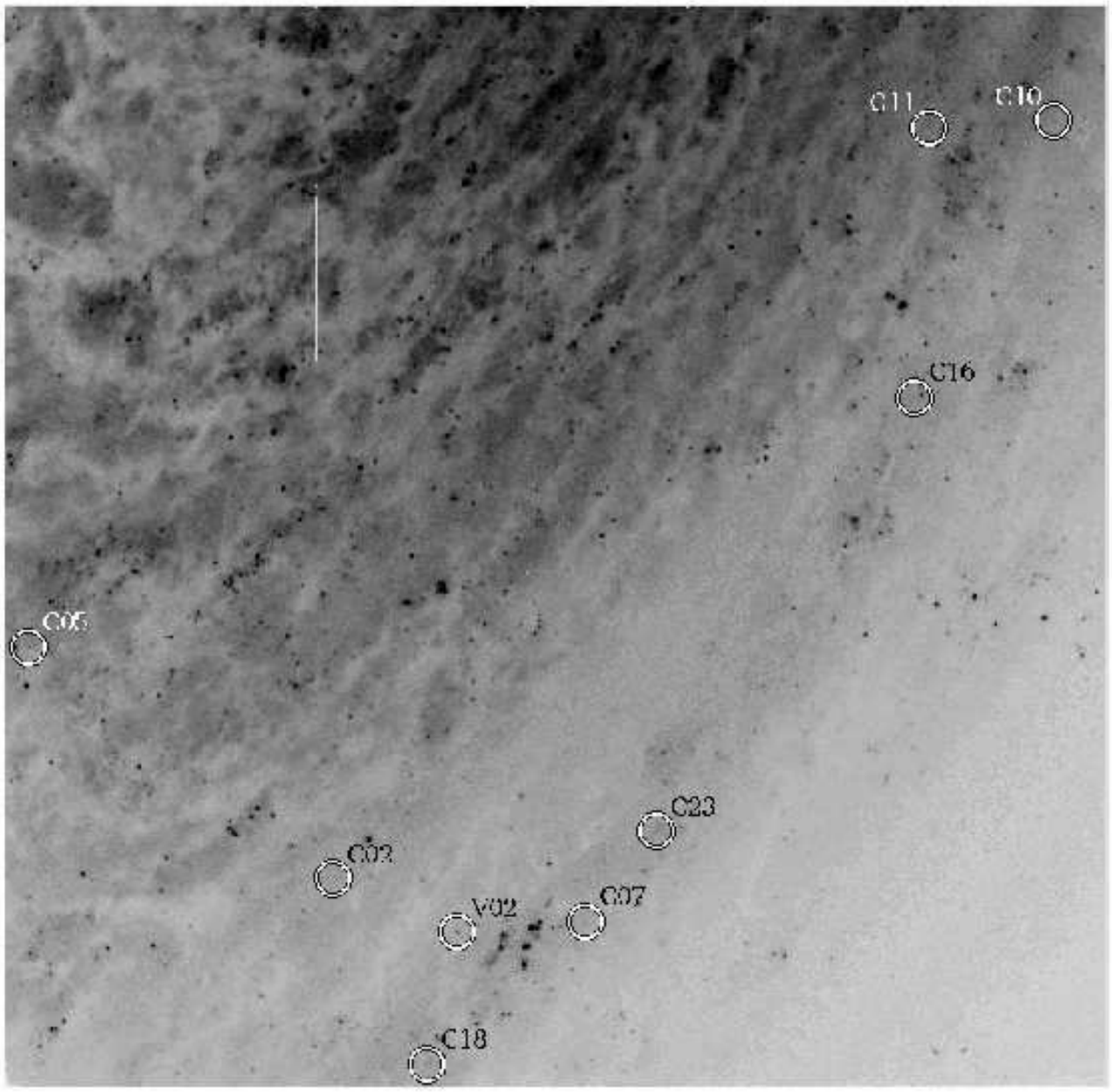

FIG. 3.— (c) continued.

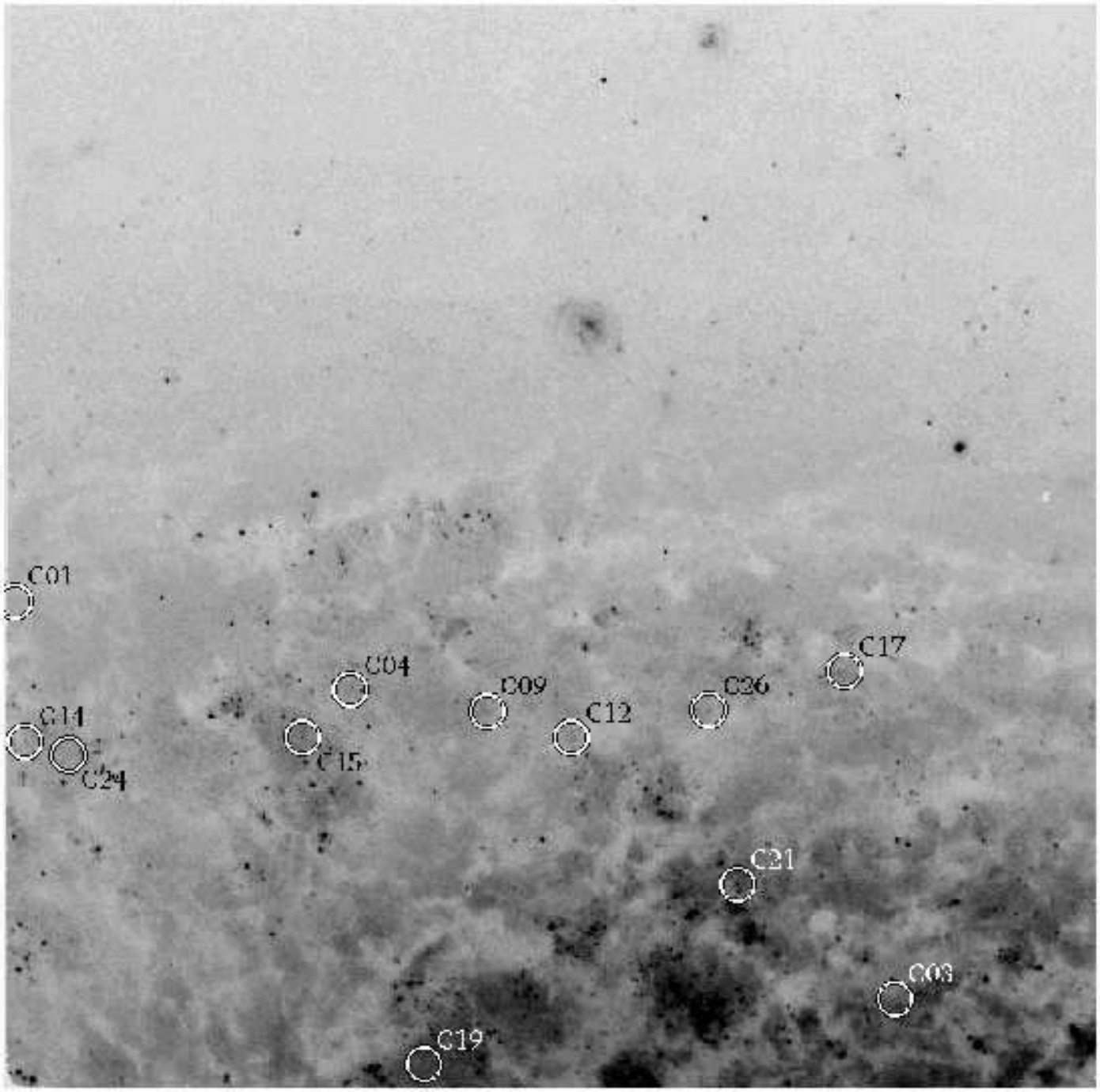

FIG. 3.— (d) continued.

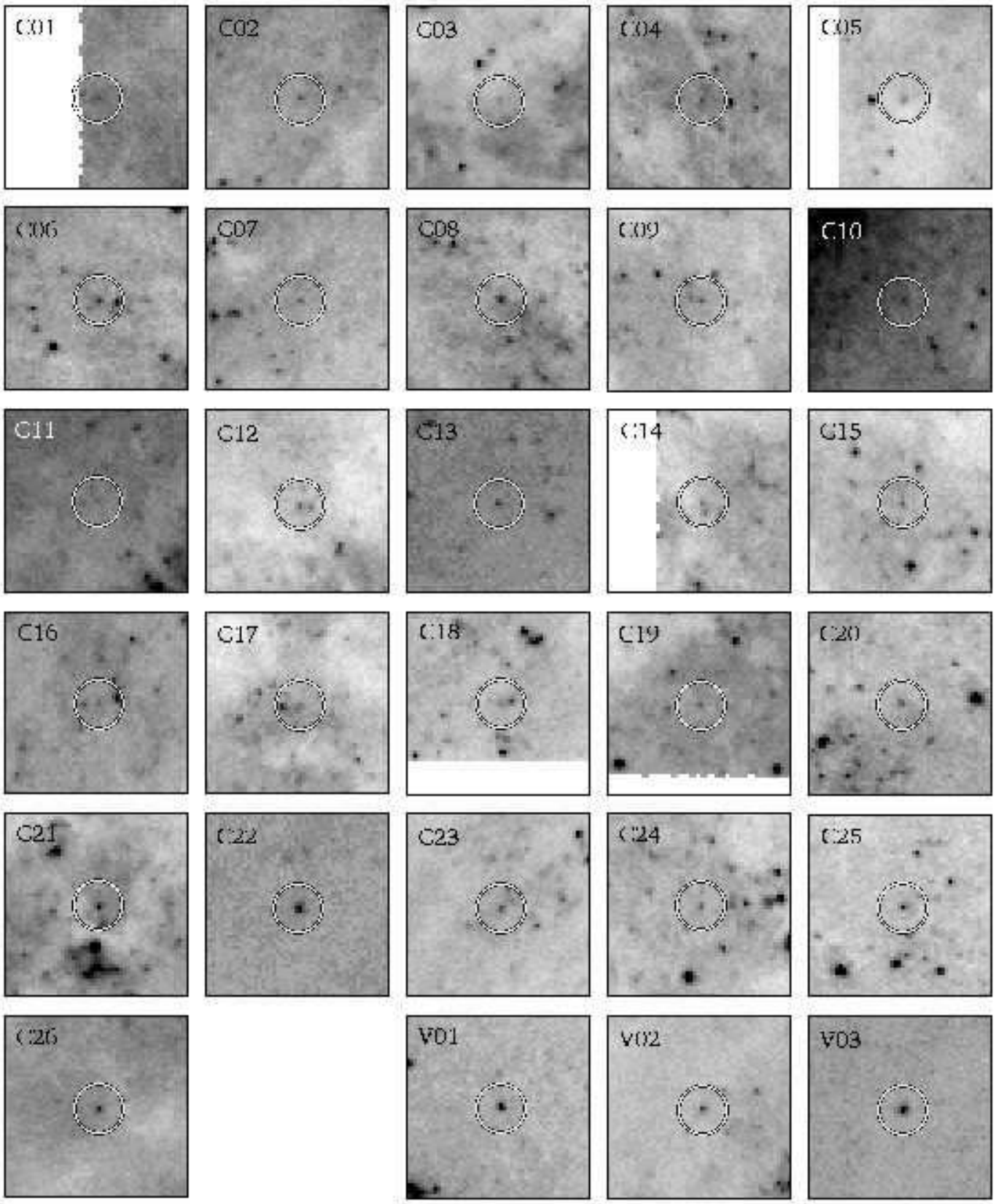

FIG. 4.— Individual finding charts for the variables. The position of each object is shown by the circle. The charts are 50 pixels on a side, i.e., $2''.15 \times 2''.15$ for objects in the PC chip and $5'' \times 5''$ for objects in the the WF chips.

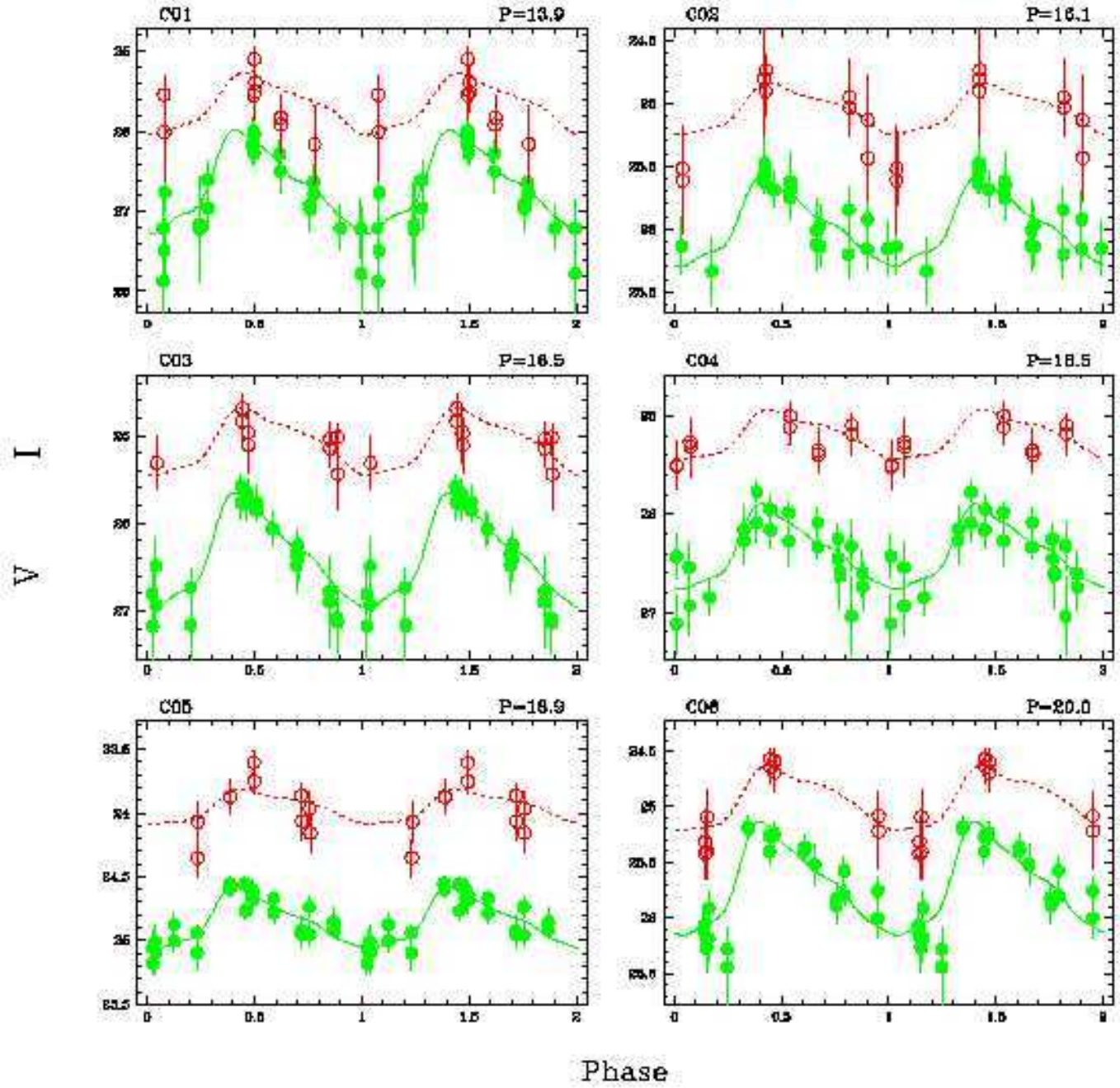

FIG. 5.— (a) V and I band phase-magnitude plots for Cepheids C01-C06. Two complete cycles are plotted to facilitate ease of interpretation. Filled and open circles are used to represent the V and I magnitudes listed in Table 5, respectively. The uncertainties associated with each measurement, also listed in that Table, are plotted using error bars. The solid and dashed lines overplotted on each panel indicate the best-fit V and I band template light curves, respectively.

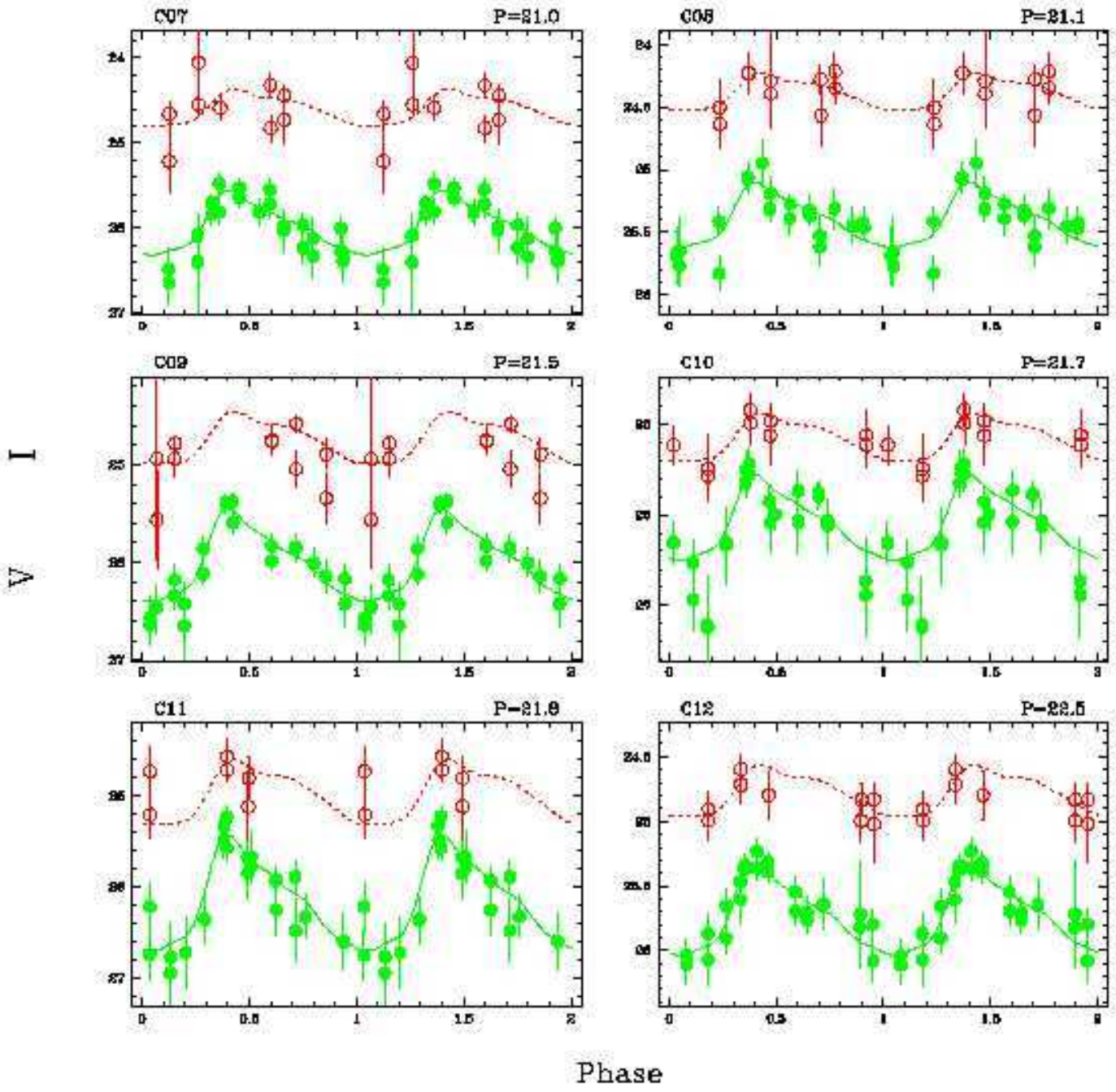

FIG. 5.— (b) same as Figure 5a, for objects C07-C12.

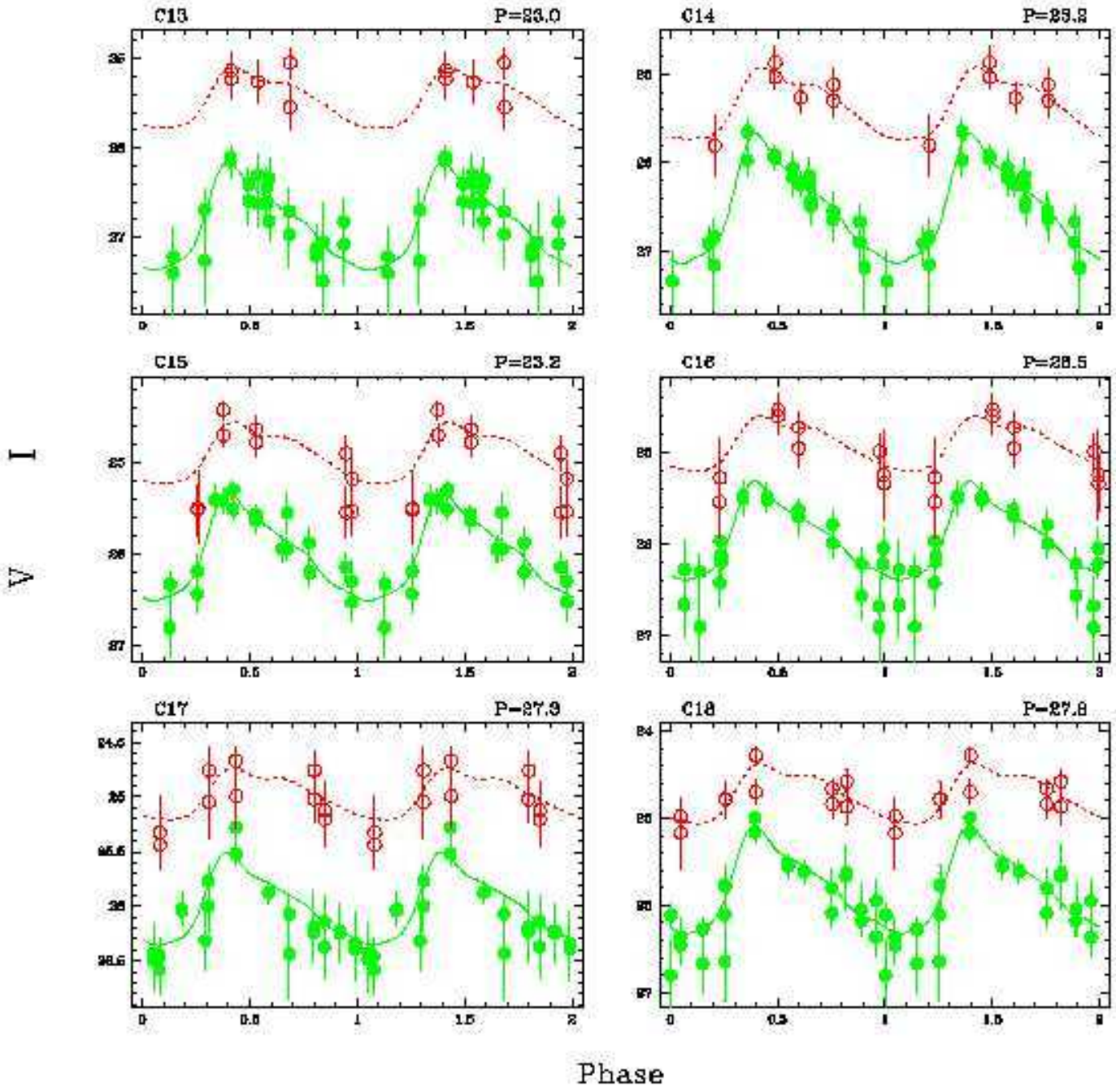

FIG. 5.— (c) same as Figure 5a, for objects C13-C18.

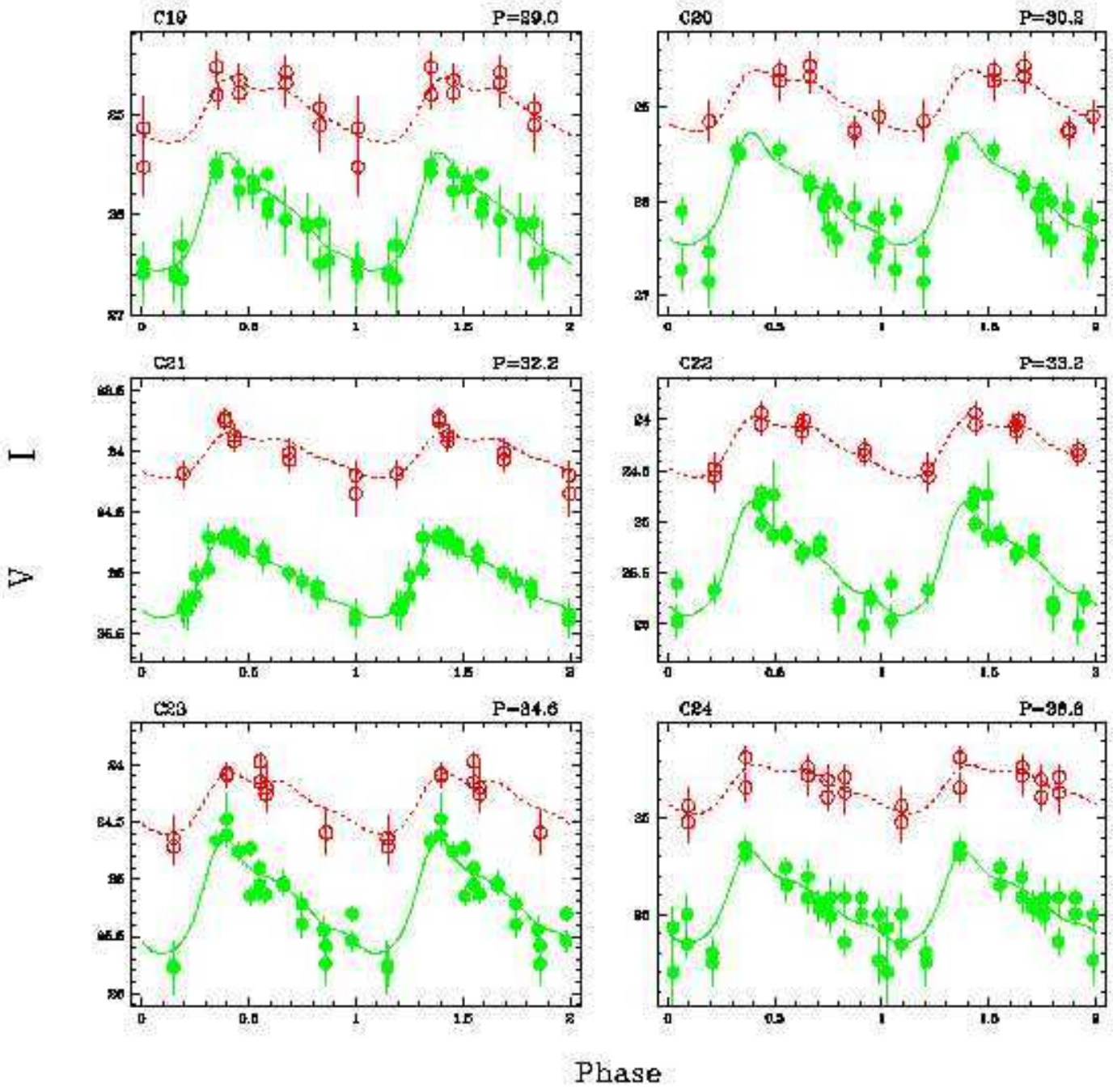

FIG. 5.— (d) same as Figure 5a, for objects C19-C24.

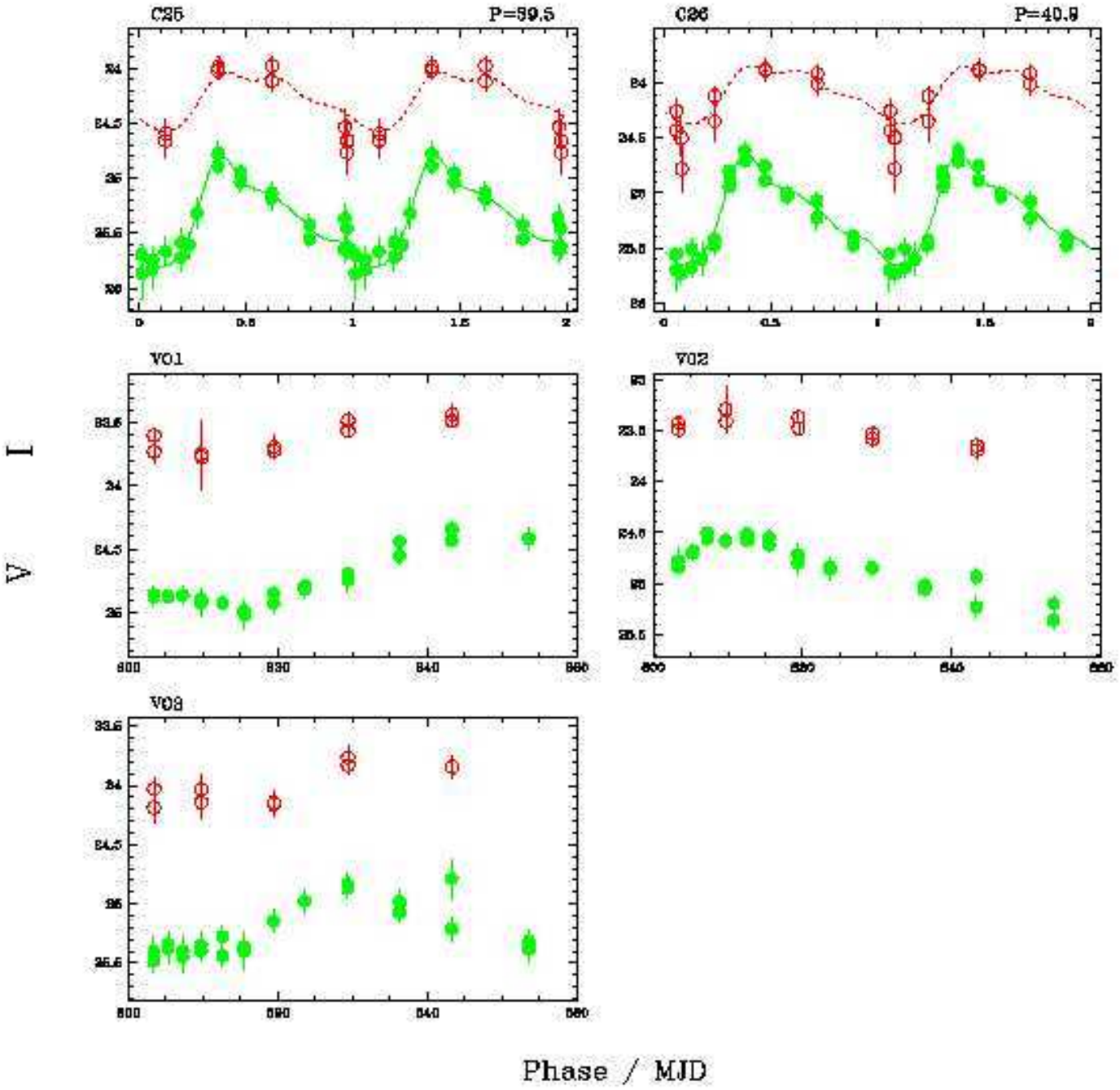

FIG. 5.— (e) Top: same as Figure 5a, for objects C25-C26. Middle and bottom: V and I band time series for the variables V01-V03, plotted as magnitude versus modified Julian Date.

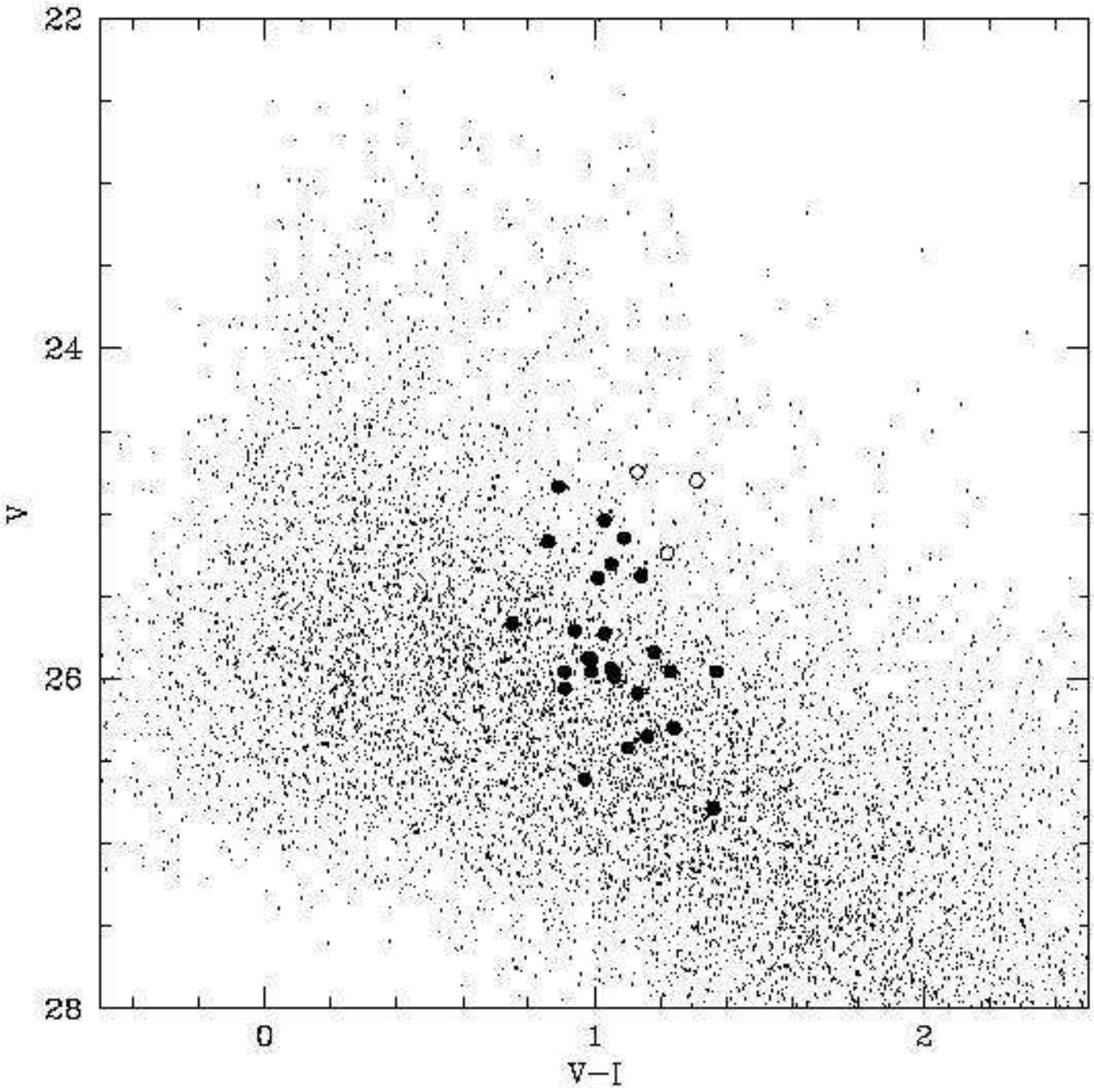

FIG. 6.— Color-magnitude diagram of the $\sim$ 9000 stars detected in our NGC 2841 images. Filled and open circles are used to plot the Cepheids and the other variables, respectively.

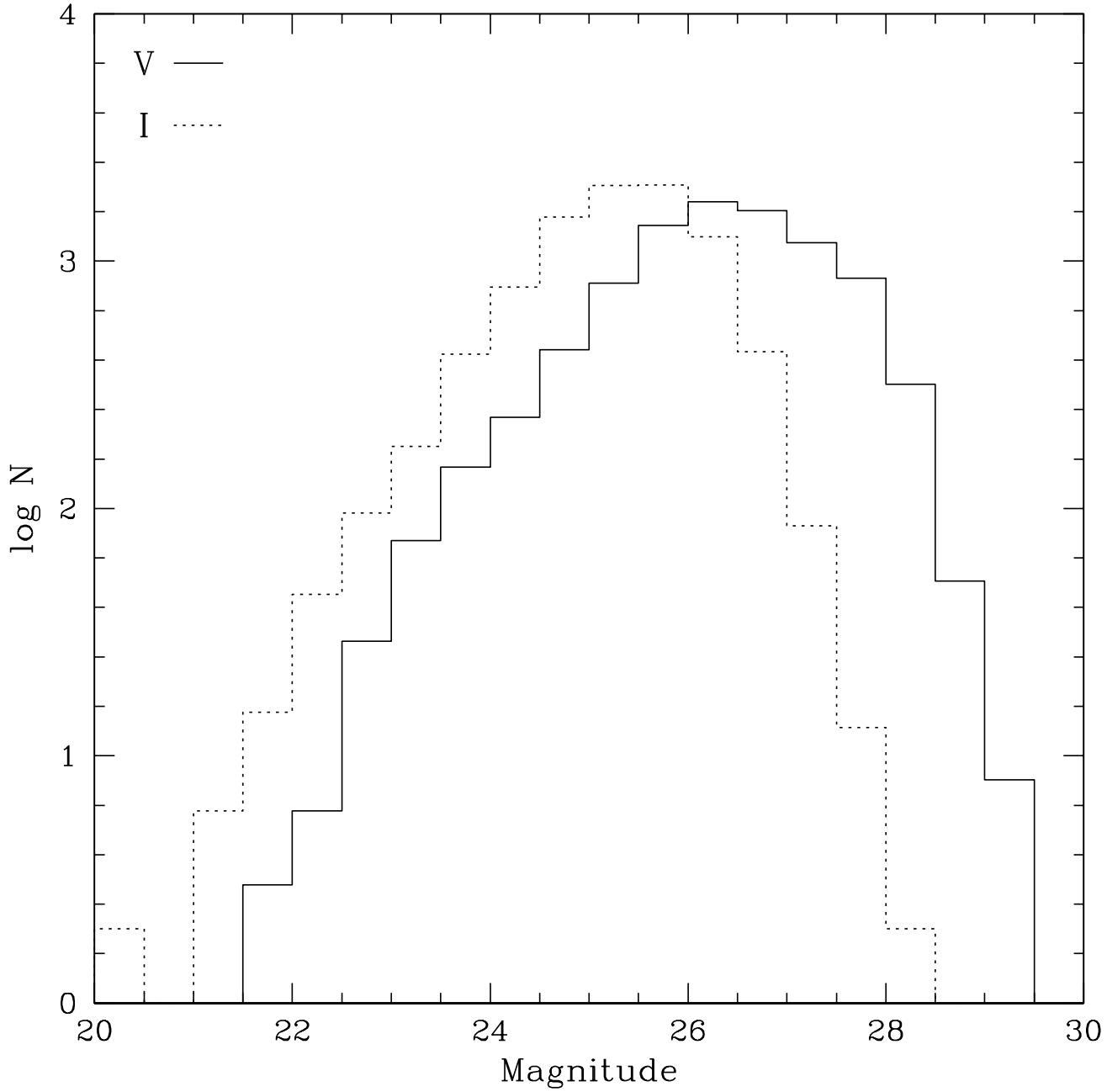

FIG. 7.— Observed differential luminosity functions in the NGC 2841 WFPC2 field. Solid and dashed lines are used to plot the V and I histograms, respectively. Based on these distributions, we determine completeness limits of V$\sim$ 26.5 mag and I$\sim$ 25.5 mag.

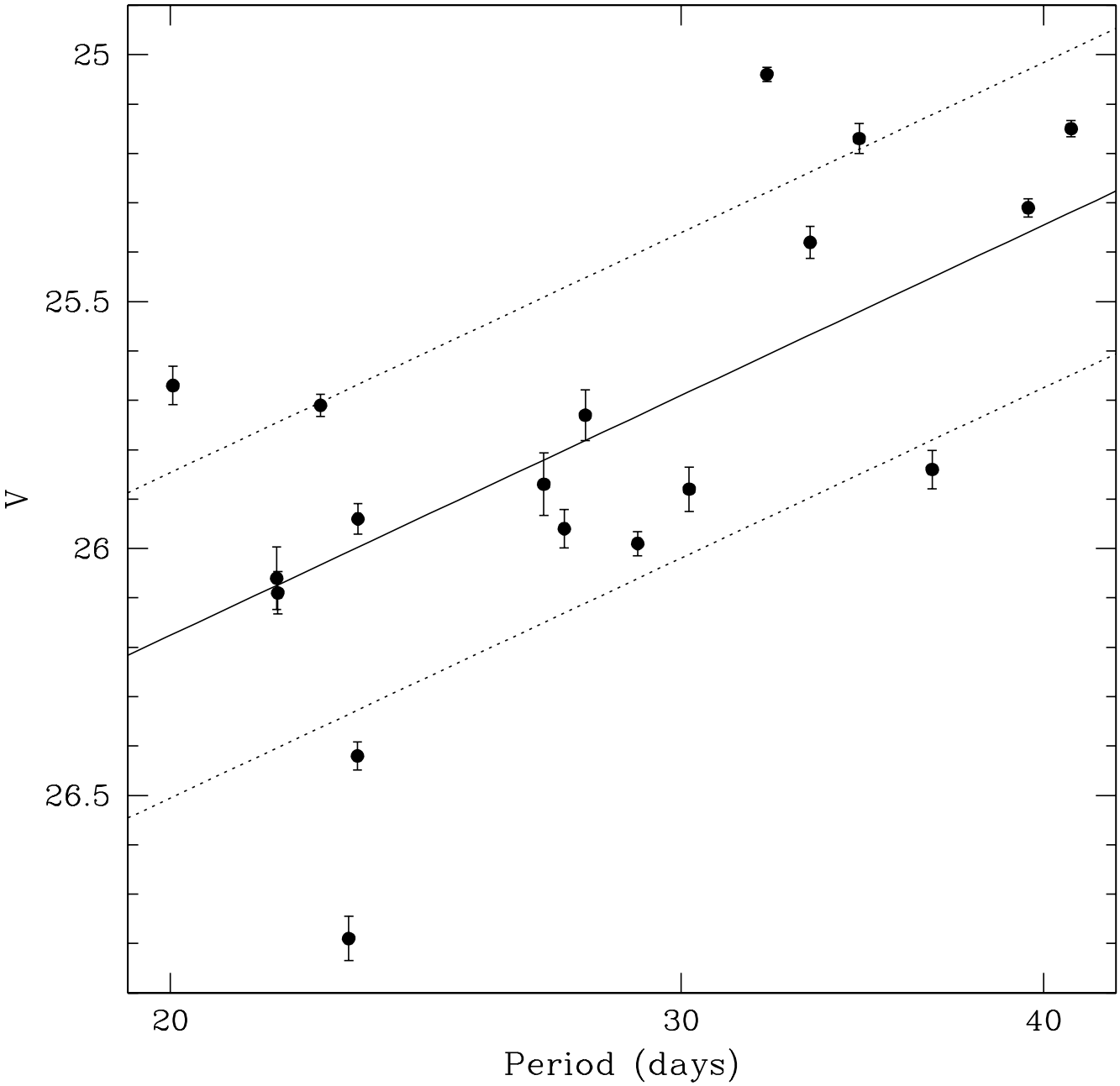

FIG. 8.— V-band Period-Luminosity relation for the selected Cepheids in our sample (see Table 4 and §5.2). The solid line is the best fit to the fiducial LMC P-L relation listed in Equation (3) and the dotted lines correspond to the *r.m.s.* dispersion of the fit. The apparent distance modulus obtained from the fit is 31.23 ± 0.08 mag.

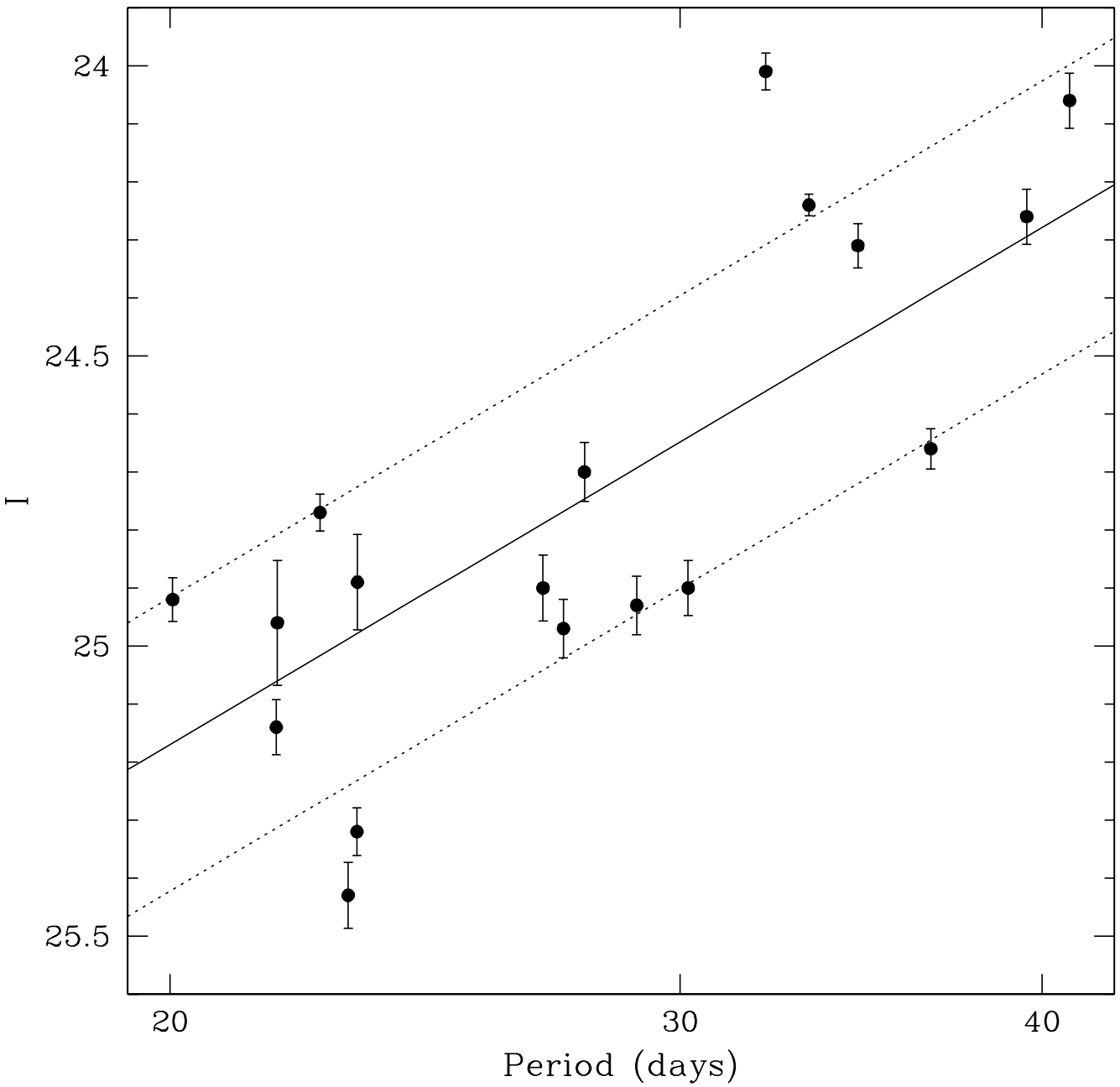

FIG. 9.— I-band Period Luminosity relation for the selected Cepheids in our sample (see Table 4 and §5.2). The solid line is the best fit to the fiducial LMC P-L relation listed in Equation (4) and the dotted lines correspond to the *r.m.s.* dispersion of the fit. The apparent distance modulus obtained from the fit is 30.96 ± 0.06 mag.

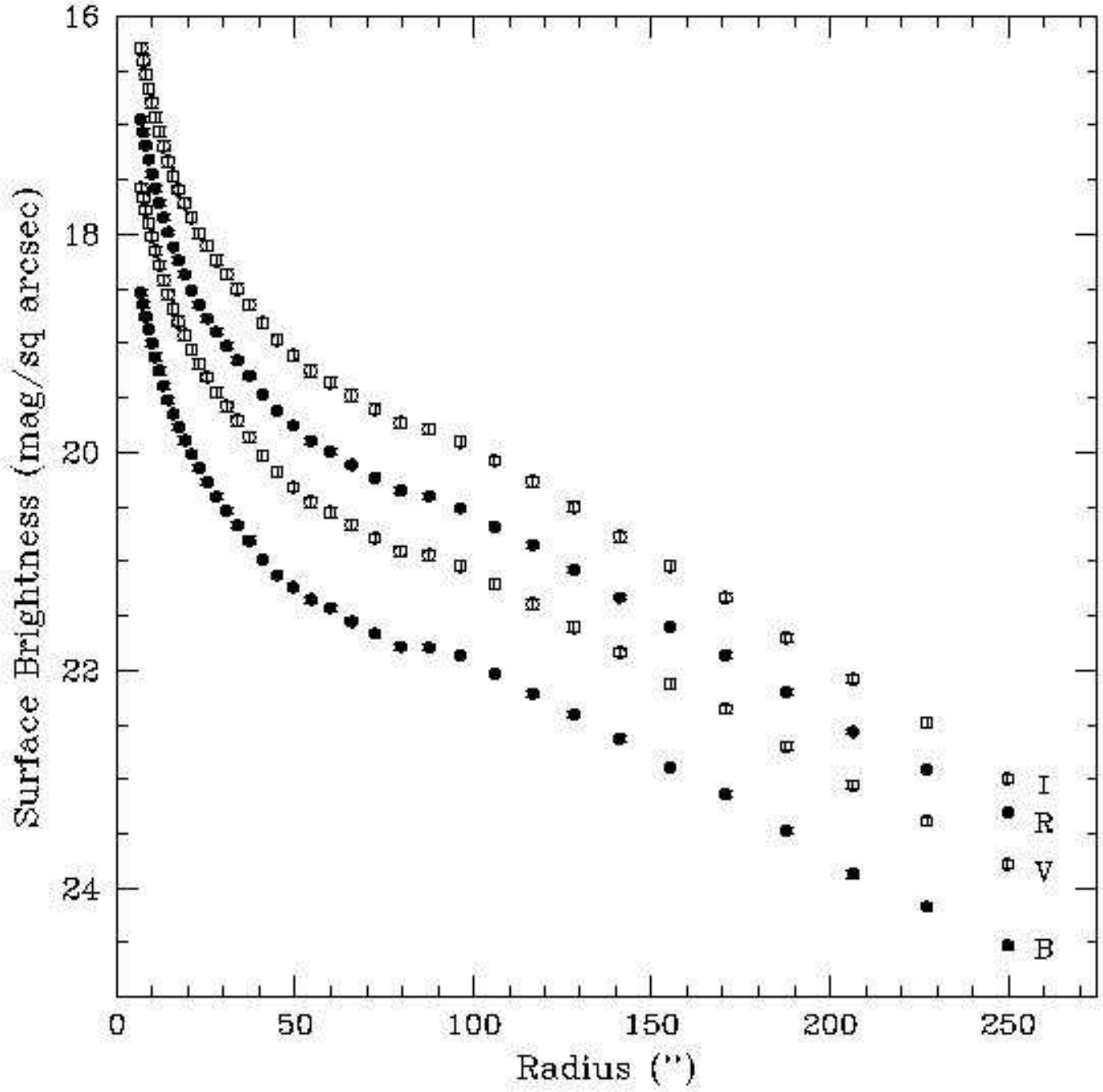

FIG. 10.— BVRI surface brightness profiles of NGC 2841, calculated from images obtained at the FLWO 1.2-m telescope and following the precepts of Macri et al. (2000).

TABLE 1
HST OBSERVATIONS OF NGC 2841

Date	JD	Exp. time	Filter
2000 Feb 29	2451603.35	$2 \times 1100s$	F555W
	2451603.41	$2 \times 1100s$	F814W
2000 Mar 02	2451605.29	$2 \times 1100s$	F555W
2000 Mar 04	2451607.24	$2 \times 1100s$	F555W
2000 Mar 06	2451609.66	$2 \times 1100s$	F555W
	2451609.72	$2 \times 1100s$	F814W
2000 Mar 09	2451612.54	$2 \times 1100s$	F555W
2000 Mar 12	2451615.49	$2 \times 1100s$	F555W
2000 Mar 16	2451619.38	$2 \times 1100s$	F555W
	2451619.44	$2 \times 1100s$	F814W
2000 Mar 20	2451623.60	$2 \times 1100s$	F555W
2000 Mar 26	2451629.30	$2 \times 1100s$	F555W
	2451629.36	$2 \times 1100s$	F814W
2000 Apr 02	2451636.27	$2 \times 1100s$	F555W
2000 Apr 09	2451643.24	$2 \times 1100s$	F555W
	2451643.31	$2 \times 1100s$	F814W
2000 Apr 19	2451653.56	$2 \times 1100s$	F555W

TABLE 2
WFPC2 ZEROPOINTS

Chip	Zeropoints	
	F555W	F814W
PC1	0.9510 ± 0.0028	1.9201 ± 0.0017
WF2	0.9584 ± 0.0016	1.8478 ± 0.0011
WF3	0.9513 ± 0.0014	1.8724 ± 0.0010
WF4	0.9697 ± 0.0015	1.9007 ± 0.0010

Table 3
Secondary standards in NGC 2841

ID	Chip	x	y	R.A. (J2000.0)	Dec.	V (mag)	I (mag)
S01	1	132.2	467.7	09:22:10.649	50:56:12.66	25.40 ± 0.02	24.55 ± 0.04
S02	1	141.4	530.3	09:22:10.725	50:56:09.88	25.26 ± 0.02	25.17 ± 0.07
S03	1	238.3	600.8	09:22:11.223	50:56:07.16	26.47 ± 0.04	24.00 ± 0.02
S04	1	540.2	144.5	09:22:12.433	50:56:29.20	25.18 ± 0.02	25.14 ± 0.10
S05	1	508.3	685.9	09:22:12.556	50:56:04.64	25.22 ± 0.02	25.23 ± 0.07
S06	1	591.2	687.4	09:22:12.952	50:56:04.99	25.84 ± 0.04	24.29 ± 0.03
S07	1	659.5	98.5	09:22:12.976	50:56:31.81	25.27 ± 0.02	25.30 ± 0.07
S08	1	715.8	262.0	09:22:13.329	50:56:24.75	24.76 ± 0.01	24.54 ± 0.06
S09	2	117.0	744.0	09:22:02.603	50:56:16.07	24.92 ± 0.02	23.20 ± 0.02
S10	2	390.5	543.7	09:22:05.010	50:55:51.50	25.28 ± 0.02	23.26 ± 0.01
S11	2	272.8	410.5	09:22:06.260	50:56:04.66	24.65 ± 0.01	23.92 ± 0.02
S12	2	193.1	396.0	09:22:06.315	50:56:12.69	24.22 ± 0.01	24.06 ± 0.02
S13	2	68.9	371.7	09:22:06.418	50:56:25.17	24.78 ± 0.01	24.07 ± 0.03
S14	2	464.0	355.9	09:22:07.063	50:55:46.39	24.52 ± 0.01	24.66 ± 0.03
S15	2	349.2	308.1	09:22:07.424	50:55:58.29	24.65 ± 0.01	24.66 ± 0.05
S16	2	189.2	271.2	09:22:07.615	50:56:14.49	24.86 ± 0.01	24.30 ± 0.03
S17	2	208.3	181.5	09:22:08.574	50:56:13.62	24.86 ± 0.02	24.20 ± 0.04
S18	2	225.7	160.3	09:22:08.816	50:56:12.14	24.50 ± 0.01	23.69 ± 0.02
S19	2	332.0	64.2	09:22:09.944	50:56:02.75	24.69 ± 0.02	24.14 ± 0.03
S20	3	730.9	495.3	09:22:02.202	50:57:07.63	24.47 ± 0.01	24.31 ± 0.04
S21	3	723.7	457.7	09:22:02.319	50:57:04.01	26.69 ± 0.06	24.08 ± 0.03
S22	3	705.2	400.4	09:22:02.576	50:56:58.57	25.38 ± 0.03	25.10 ± 0.09
S23	3	716.0	214.2	09:22:02.682	50:56:40.13	25.19 ± 0.02	24.92 ± 0.07
S24	3	689.1	373.8	09:22:02.774	50:56:56.12	26.39 ± 0.07	24.26 ± 0.04
S25	3	702.8	156.2	09:22:02.888	50:56:34.59	26.83 ± 0.07	24.14 ± 0.03
S26	3	631.8	364.0	09:22:03.382	50:56:55.77	23.78 ± 0.01	22.80 ± 0.02
S27	3	634.1	284.6	09:22:03.450	50:56:47.92	24.44 ± 0.01	24.11 ± 0.03
S28	3	607.5	139.7	09:22:03.897	50:56:33.96	25.09 ± 0.01	22.40 ± 0.02
S29	3	509.6	207.4	09:22:04.840	50:56:41.64	26.46 ± 0.06	24.30 ± 0.03
S30	3	473.9	177.8	09:22:05.247	50:56:39.12	23.22 ± 0.01	22.34 ± 0.01
S31	3	462.7	101.3	09:22:05.452	50:56:31.73	24.77 ± 0.02	24.83 ± 0.06
S32	3	434.2	248.7	09:22:05.580	50:56:46.53	27.02 ± 0.07	23.91 ± 0.02
S33	3	425.0	225.3	09:22:05.704	50:56:44.32	26.31 ± 0.04	24.42 ± 0.04
S34	3	385.3	100.9	09:22:06.261	50:56:32.52	24.48 ± 0.01	24.24 ± 0.03
S35	3	360.1	82.5	09:22:06.545	50:56:31.00	26.07 ± 0.03	23.60 ± 0.02
S36	3	282.6	110.9	09:22:07.322	50:56:34.63	26.55 ± 0.06	23.91 ± 0.02
S37	3	280.5	93.6	09:22:07.363	50:56:32.96	25.19 ± 0.02	24.77 ± 0.05
S38	3	249.9	78.8	09:22:07.698	50:56:31.85	25.15 ± 0.02	24.64 ± 0.05
S39	3	220.4	141.7	09:22:07.936	50:56:38.34	24.75 ± 0.01	24.45 ± 0.04
S40	3	163.9	162.4	09:22:08.500	50:56:41.01	24.85 ± 0.02	24.32 ± 0.03
S41	4	85.5	262.1	09:22:12.214	50:56:37.22	23.26 ± 0.01	22.95 ± 0.02
S42	4	588.9	323.0	09:22:12.322	50:57:27.53	24.52 ± 0.01	24.49 ± 0.03
S43	4	296.7	300.6	09:22:12.392	50:56:58.40	23.90 ± 0.01	23.80 ± 0.01
S44	4	132.5	309.9	09:22:12.663	50:56:42.30	25.08 ± 0.02	24.58 ± 0.04
S45	4	202.5	371.4	09:22:13.233	50:56:49.80	24.41 ± 0.01	23.06 ± 0.01
S46	4	502.3	421.4	09:22:13.443	50:57:19.95	23.95 ± 0.01	23.58 ± 0.02
S47	4	154.1	389.7	09:22:13.476	50:56:45.21	24.79 ± 0.01	24.72 ± 0.03
S48	4	257.2	420.9	09:22:13.695	50:56:55.69	22.80 ± 0.01	21.97 ± 0.01
S49	4	229.0	439.2	09:22:13.916	50:56:53.09	24.83 ± 0.02	24.37 ± 0.03
S50	4	684.1	510.6	09:22:14.185	50:57:38.74	24.76 ± 0.01	24.65 ± 0.03
S51	4	738.3	543.7	09:22:14.473	50:57:44.37	24.76 ± 0.01	24.31 ± 0.03
S52	4	595.7	535.8	09:22:14.543	50:57:30.30	26.11 ± 0.05	23.25 ± 0.01
S53	4	507.6	545.1	09:22:14.733	50:57:21.69	24.94 ± 0.02	24.06 ± 0.05

TABLE 3—*Continued*

ID	Chip	x	y	R.A. (J2000.0)	Dec.	V (mag)	I (mag)
S54	4	595.3	562.4	09:22:14.821	50:57:30.52	24.66 ± 0.01	24.06 ± 0.02
S55	4	722.2	577.1	09:22:14.838	50:57:43.11	24.57 ± 0.01	23.54 ± 0.02
S56	4	752.0	587.9	09:22:14.919	50:57:46.12	24.44 ± 0.01	24.10 ± 0.02
S57	4	157.4	539.7	09:22:15.042	50:56:47.04	23.71 ± 0.01	23.39 ± 0.02
S58	4	131.8	652.5	09:22:16.243	50:56:45.68	25.90 ± 0.03	23.45 ± 0.01
S59	4	662.6	737.1	09:22:16.565	50:57:38.77	23.54 ± 0.01	22.82 ± 0.01
S60	4	481.2	718.5	09:22:16.569	50:57:20.77	24.85 ± 0.01	23.93 ± 0.02
S61	4	459.2	747.9	09:22:16.897	50:57:18.89	23.49 ± 0.01	22.94 ± 0.01

TABLE 4
VARIABLES DISCOVERED IN NGC 2841

ID	Chip	x	y	R.A. (J2000.0)	Dec.	P (d)	V (mag)	I (mag)	
C01	4	51.7	387.2	09:22:13.556	+50:56:35.13	13.9 ± 0.6	26.61 ± 0.05	25.64 ± 0.11	
C02	3	263.2	194.9	09:22:07.430	+50:56:43.10	16.1 ± 0.5	25.96 ± 0.03	25.05 ± 0.06	
C03	4	660.6	112.5	09:22:10.055	+50:57:32.45	16.5 ± 0.2	26.30 ± 0.04	25.06 ± 0.07	
C04	4	284.2	325.8	09:22:12.669	+50:56:57.42	18.5 ± 0.5	26.35 ± 0.04	25.19 ± 0.05	
C05	3	52.3	355.3	09:22:09.441	+50:57:01.23	18.9 ± 0.6	24.84 ± 0.02	23.95 ± 0.05	
C06	2	111.0	118.1	09:22:09.112	+50:56:23.87	20.0 ± 0.3	25.67 ± 0.04	24.92 ± 0.04	*
C07	3	438.1	165.2	09:22:05.636	+50:56:38.26	21.0 ± 0.4	25.96 ± 0.03	24.59 ± 0.11	
C08	2	129.0	102.3	09:22:09.298	+50:56:22.28	21.1 ± 1.1	25.39 ± 0.03	24.38 ± 0.04	
C09	4	378.8	311.1	09:22:12.416	+50:57:06.63	21.5 ± 0.5	25.96 ± 0.03	24.73 ± 0.09	
C10	3	762.2	719.8	09:22:01.632	+50:57:29.27	21.7 ± 1.0	26.06 ± 0.06	25.15 ± 0.05	*
C11	3	675.6	715.4	09:22:02.530	+50:57:29.84	21.8 ± 0.7	26.09 ± 0.05	24.96 ± 0.14	*
C12	4	437.0	292.6	09:22:12.161	+50:57:12.21	22.5 ± 0.3	25.71 ± 0.02	24.77 ± 0.03	*
C13	1	382.6	145.9	09:22:11.681	+50:56:28.38	23.0 ± 0.8	26.79 ± 0.05	25.43 ± 0.08	*
C14	4	59.4	290.3	09:22:12.536	+50:56:34.94	23.2 ± 0.4	26.42 ± 0.03	25.32 ± 0.05	*
C15	4	251.0	293.2	09:22:12.363	+50:56:53.81	23.2 ± 0.3	25.94 ± 0.03	24.89 ± 0.08	*
C16	3	666.2	528.2	09:22:02.836	+50:57:11.58	26.5 ± 0.8	25.88 ± 0.05	24.89 ± 0.06	*
C17	4	626.0	338.8	09:22:12.449	+50:57:31.34	27.3 ± 1.0	25.96 ± 0.04	24.97 ± 0.05	*
C18	3	328.2	66.4	09:22:06.896	+50:56:29.77	27.8 ± 0.6	25.73 ± 0.05	24.70 ± 0.05	*
C19	4	334.8	66.9	09:22:09.914	+50:56:59.89	29.0 ± 0.9	25.99 ± 0.03	24.93 ± 0.05	*
C20	2	253.8	75.2	09:22:09.735	+50:56:10.33	30.2 ± 0.5	25.88 ± 0.05	24.90 ± 0.05	*
C21	4	551.9	191.4	09:22:10.985	+50:57:22.56	32.2 ± 0.7	25.04 ± 0.01	24.01 ± 0.03	*
C22	1	689.7	435.7	09:22:13.295	+50:56:16.80	33.2 ± 0.8	25.38 ± 0.03	24.24 ± 0.02	*
C23	3	487.1	227.6	09:22:05.051	+50:56:43.88	34.6 ± 1.4	25.17 ± 0.03	24.31 ± 0.04	*
C24	4	88.9	281.4	09:22:12.412	+50:56:37.74	36.6 ± 1.8	25.84 ± 0.04	24.66 ± 0.03	*
C25	2	291.2	93.9	09:22:09.587	+50:56:06.44	39.5 ± 0.8	25.31 ± 0.02	24.26 ± 0.05	*
C26	4	532.1	311.9	09:22:12.264	+50:57:21.81	40.9 ± 0.5	25.15 ± 0.02	24.06 ± 0.05	*
V01	2	218.2	384.2	09:22:06.469	+50:56:10.35	...	24.75 ± 0.04	23.62 ± 0.04	
V02	3	349.3	157.6	09:22:06.573	+50:56:38.48	...	24.80 ± 0.05	23.49 ± 0.04	
V03	1	460.2	188.6	09:22:12.073	+50:56:26.84	...	25.24 ± 0.04	24.02 ± 0.05	

Note. — (*): Variable was used to construct the P-L relations shown in Figures 8 and 9.

Table 5
Individual V band photometric measurements

MJD	Variables				
	C01	C02	C03	C04	C05
603.36	26.28 ± 0.16	25.48 ± 0.21	25.74 ± 0.12	26.33 ± 0.13	24.55 ± 0.04
603.38	26.50 ± 0.28	25.53 ± 0.14	25.66 ± 0.16	26.09 ± 0.16	24.60 ± 0.06
605.30	26.91 ± 0.34	25.69 ± 0.14	26.06 ± 0.20	26.59 ± 0.38	24.66 ± 0.13
605.32	26.98 ± 0.23	25.64 ± 0.16	26.07 ± 0.17	26.63 ± 0.21	24.60 ± 0.09
607.25	...	26.13 ± 0.20	26.25 ± 0.18	26.60 ± 0.24	24.67 ± 0.05
607.26	27.21 ± 0.28	26.02 ± 0.25	26.40 ± 0.24	26.74 ± 0.24	24.79 ± 0.08
609.67	27.21 ± 0.36	26.20 ± 0.20	26.78 ± 0.22	26.43 ± 0.22	24.95 ± 0.06
609.68	27.88 ± 0.68	25.85 ± 0.18	26.90 ± 0.52	27.11 ± 0.30	24.93 ± 0.13
612.55	26.61 ± 0.24	...	26.80 ± 0.27	...	24.92 ± 0.06
612.56	26.95 ± 0.27	26.16 ± 0.22	27.18 ± 0.55	26.84 ± 0.19	24.85 ± 0.11
615.50	26.00 ± 0.16	26.34 ± 0.26	26.73 ± 0.22	26.27 ± 0.23	25.18 ± 0.09
615.51	26.01 ± 0.19	...	27.16 ± 0.46	26.16 ± 0.24	25.06 ± 0.15
619.39	26.64 ± 0.22	25.57 ± 0.14	25.57 ± 0.11	26.27 ± 0.25	24.94 ± 0.06
619.40	26.78 ± 0.24	25.63 ± 0.08	25.77 ± 0.19	25.98 ± 0.12	25.10 ± 0.13
623.61	27.49 ± 0.38	25.97 ± 0.15	26.36 ± 0.16	26.25 ± 0.15	24.55 ± 0.05
623.62	26.76 ± 0.24	26.14 ± 0.15	26.48 ± 0.31	26.45 ± 0.25	24.77 ± 0.06
629.31	26.18 ± 0.22	...	26.49 ± 0.31	26.54 ± 0.26	24.74 ± 0.08
629.32	26.14 ± 0.19	26.14 ± 0.23	26.93 ± 0.30	26.93 ± 0.31	24.96 ± 0.09
636.28	27.21 ± 0.37	25.69 ± 0.13	25.79 ± 0.17	26.16 ± 0.18	24.87 ± 0.09
636.29	27.78 ± 0.84	...	25.77 ± 0.15	25.95 ± 0.15	25.00 ± 0.08
643.25	26.27 ± 0.13	26.16 ± 0.17	27.08 ± 0.35	26.32 ± 0.26	24.68 ± 0.10
643.27	26.03 ± 0.12	25.92 ± 0.22	27.14 ± 0.36	27.04 ± 0.41	24.65 ± 0.11
653.57	27.16 ± 0.52	25.75 ± 0.17	25.86 ± 0.11	26.09 ± 0.19	25.01 ± 0.12
653.59	27.23 ± 0.66	25.62 ± 0.23	25.76 ± 0.20	25.77 ± 0.10	25.09 ± 0.17
	C06	C07	C08	C09	C10
603.36	26.27 ± 0.22	25.81 ± 0.15	25.32 ± 0.10	...	27.21 ± 0.52
603.38	26.19 ± 0.17	25.48 ± 0.12	25.19 ± 0.14	26.14 ± 0.17	27.24 ± 0.39
605.30	26.44 ± 0.35	25.64 ± 0.10	25.39 ± 0.14	26.42 ± 0.23	26.30 ± 0.23
605.32	26.29 ± 0.16	25.53 ± 0.11	25.28 ± 0.07	26.16 ± 0.15	26.34 ± 0.43
607.25	25.18 ± 0.10	25.82 ± 0.09	25.33 ± 0.12	26.57 ± 0.22	25.65 ± 0.16
607.26	25.20 ± 0.11	25.81 ± 0.15	25.37 ± 0.07	26.64 ± 0.20	25.50 ± 0.20
609.67	25.25 ± 0.06	26.02 ± 0.24	25.31 ± 0.16	26.34 ± 0.13	25.86 ± 0.15
609.68	25.24 ± 0.10	25.98 ± 0.15	...	26.18 ± 0.17	26.09 ± 0.32
612.55	25.36 ± 0.11	26.12 ± 0.25	25.43 ± 0.12	25.86 ± 0.13	25.74 ± 0.21
612.56	25.39 ± 0.11	26.33 ± 0.24	25.46 ± 0.07	26.12 ± 0.12	26.08 ± 0.35
615.50	25.82 ± 0.14	26.39 ± 0.26	25.77 ± 0.16	25.38 ± 0.09	26.07 ± 0.17
615.51	25.89 ± 0.15	26.32 ± 0.23	25.65 ± 0.27	25.59 ± 0.11	26.12 ± 0.28
619.39	25.76 ± 0.13	26.49 ± 0.25	25.42 ± 0.11	25.83 ± 0.12	26.73 ± 0.46
619.40	26.00 ± 0.17	26.64 ± 0.24	25.83 ± 0.13	25.98 ± 0.10	26.88 ± 0.47
623.61	26.18 ± 0.21	25.71 ± 0.10	24.95 ± 0.19	26.01 ± 0.12	26.53 ± 0.24
623.62	25.91 ± 0.15	25.84 ± 0.14	24.95 ± 0.12	26.00 ± 0.14	26.94 ± 0.33
629.31	25.27 ± 0.09	25.55 ± 0.12	25.53 ± 0.16	26.46 ± 0.25	25.55 ± 0.18
629.32	25.40 ± 0.13	25.72 ± 0.16	25.62 ± 0.15	26.44 ± 0.18	25.44 ± 0.18
636.28	25.58 ± 0.13	26.27 ± 0.20	25.69 ± 0.20	25.40 ± 0.10	25.79 ± 0.14
636.29	25.80 ± 0.10	26.00 ± 0.13	25.69 ± 0.23	25.38 ± 0.08	25.77 ± 0.13
643.25	26.13 ± 0.20	26.09 ± 0.20	25.08 ± 0.07	25.86 ± 0.16	26.32 ± 0.23
643.27	26.07 ± 0.12	26.40 ± 0.58	25.06 ± 0.12	25.84 ± 0.14	26.30 ± 0.23
653.57	25.52 ± 0.18	25.96 ± 0.13	25.45 ± 0.15	26.65 ± 0.36	26.00 ± 0.17
653.59	...	26.23 ± 0.20	...	26.43 ± 0.23	...
	C11	C12	C13	C14	C15
603.36	...	25.87 ± 0.15	26.15 ± 0.18	25.95 ± 0.13	26.19 ± 0.19
603.38	26.72 ± 0.39	26.07 ± 0.20	26.10 ± 0.12	25.92 ± 0.10	26.44 ± 0.21

TABLE 5—*Continued*

MJD	Variables				
605.30	26.36 ± 0.26	25.90 ± 0.12	26.59 ± 0.26	26.17 ± 0.21	25.40 ± 0.15
605.32	...	25.65 ± 0.14	26.40 ± 0.17	26.05 ± 0.18	25.42 ± 0.16
607.25	25.33 ± 0.11	25.34 ± 0.08	26.43 ± 0.22	26.50 ± 0.20	25.30 ± 0.08
607.26	25.48 ± 0.20	25.38 ± 0.07	26.61 ± 0.19	26.44 ± 0.26	25.30 ± 0.08
609.67	25.68 ± 0.16	25.39 ± 0.08	26.71 ± 0.26	26.54 ± 0.22	25.56 ± 0.10
609.68	25.85 ± 0.28	25.32 ± 0.08	26.97 ± 0.37	26.64 ± 0.25	25.64 ± 0.15
612.55	25.93 ± 0.14	25.70 ± 0.11	27.12 ± 0.23	26.90 ± 0.29	25.95 ± 0.13
612.56	26.25 ± 0.27	25.55 ± 0.13	27.20 ± 0.34	26.66 ± 0.20	25.94 ± 0.15
615.50	26.33 ± 0.23	25.64 ± 0.20	27.08 ± 0.45	...	25.87 ± 0.16
615.51	...	25.65 ± 0.14	26.83 ± 0.26	27.34 ± 0.35	26.20 ± 0.16
619.39	26.60 ± 0.31	25.82 ± 0.13	...	26.91 ± 0.20	...
619.40	...	25.72 ± 0.41	...	...	26.15 ± 0.17
623.61	26.95 ± 0.34	26.04 ± 0.12	26.70 ± 0.24	25.97 ± 0.19	26.80 ± 0.34
623.62	26.77 ± 0.38	26.11 ± 0.14	27.26 ± 0.48	25.65 ± 0.15	26.33 ± 0.12
629.31	25.23 ± 0.13	25.47 ± 0.07	26.30 ± 0.23	26.22 ± 0.12	25.42 ± 0.14
629.32	25.57 ± 0.14	25.60 ± 0.19	26.61 ± 0.27	26.24 ± 0.14	25.41 ± 0.06
636.28	25.89 ± 0.19	25.77 ± 0.09	27.49 ± 0.40	27.19 ± 0.50	25.55 ± 0.22
636.29	26.48 ± 0.35	25.71 ± 0.12	27.05 ± 0.44	27.17 ± 0.29	25.94 ± 0.12
643.25	26.75 ± 0.27	26.08 ± 0.17	27.40 ± 0.46	27.16 ± 0.51	26.30 ± 0.22
643.27	26.22 ± 0.27	25.80 ± 0.12	27.22 ± 0.34	26.84 ± 0.22	26.53 ± 0.22
653.57	25.66 ± 0.28	25.23 ± 0.10	26.34 ± 0.24	26.15 ± 0.19	25.31 ± 0.10
653.59	25.77 ± 0.18	25.36 ± 0.09	26.82 ± 0.23	26.25 ± 0.17	25.51 ± 0.11
	C16	C17	C18	C19	C20
603.36	26.22 ± 0.16	26.14 ± 0.23	25.68 ± 0.38	25.58 ± 0.12	25.84 ± 0.15
603.38	26.05 ± 0.23	26.37 ± 0.29	25.63 ± 0.14	25.76 ± 0.19	25.78 ± 0.11
605.30	26.67 ± 0.35	26.25 ± 0.28	26.19 ± 0.17	25.66 ± 0.14	26.00 ± 0.10
605.32	26.28 ± 0.32	26.22 ± 0.15	26.05 ± 0.31	25.74 ± 0.18	26.05 ± 0.20
607.25	26.30 ± 0.19	26.39 ± 0.30	26.36 ± 0.23	25.60 ± 0.06	26.40 ± 0.18
607.26	26.91 ± 0.39	26.34 ± 0.29	25.95 ± 0.25	25.98 ± 0.16	25.99 ± 0.11
609.67	26.43 ± 0.27	26.46 ± 0.18	26.36 ± 0.16	...	26.06 ± 0.25
609.68	25.96 ± 0.15	26.58 ± 0.23	26.46 ± 0.23	26.05 ± 0.35	26.05 ± 0.18
612.55	25.47 ± 0.10	26.04 ± 0.11	26.27 ± 0.13	26.12 ± 0.34	26.59 ± 0.22
612.56	25.50 ± 0.18	26.02 ± 0.16	26.67 ± 0.34	26.09 ± 0.14	26.17 ± 0.10
615.50	25.52 ± 0.13	...	25.77 ± 0.24	...	26.72 ± 0.23
615.51	25.48 ± 0.15	26.31 ± 0.27	25.78 ± 0.15	26.46 ± 0.39	26.09 ± 0.14
619.39	25.70 ± 0.20	25.28 ± 0.18	25.00 ± 0.07	26.59 ± 0.30	26.53 ± 0.23
619.40	25.62 ± 0.09	25.52 ± 0.11	25.16 ± 0.12	26.48 ± 0.21	26.84 ± 0.28
623.61	25.79 ± 0.17	25.88 ± 0.10	25.55 ± 0.14	26.62 ± 0.21	25.46 ± 0.07
623.62	26.00 ± 0.15	...	25.52 ± 0.09	26.58 ± 0.29	25.50 ± 0.12
629.31	26.68 ± 0.32	26.24 ± 0.22	26.09 ± 0.18	25.50 ± 0.12	25.45 ± 0.11
629.32	26.91 ± 0.47	26.19 ± 0.32	25.80 ± 0.21	25.57 ± 0.11	...
636.28	26.20 ± 0.15	26.43 ± 0.27	26.80 ± 0.41	...	25.86 ± 0.11
636.29	26.13 ± 0.18	26.49 ± 0.27	26.11 ± 0.13	25.88 ± 0.10	26.29 ± 0.19
643.25	...	25.77 ± 0.15	26.65 ± 0.45	26.49 ± 0.17	26.45 ± 0.22
643.27	...	26.00 ± 0.25	26.10 ± 0.18	26.08 ± 0.16	26.18 ± 0.21
653.57	26.22 ± 0.17	26.07 ± 0.18	25.61 ± 0.13	26.30 ± 0.25	25.45 ± 0.14
653.59	26.57 ± 0.26	26.43 ± 0.42	...	26.65 ± 0.34	...
	C21	C22	C23	C24	C25
603.36	25.29 ± 0.09	25.02 ± 0.07	24.62 ± 0.09	25.82 ± 0.16	25.65 ± 0.12
603.38	25.29 ± 0.15	24.71 ± 0.09	24.48 ± 0.22	25.61 ± 0.17	25.36 ± 0.14
605.30	25.19 ± 0.10	24.74 ± 0.34	24.76 ± 0.07	25.94 ± 0.13	25.69 ± 0.09
605.32	25.02 ± 0.12	25.13 ± 0.09	...	25.89 ± 0.14	25.87 ± 0.22
607.25	24.97 ± 0.08	25.10 ± 0.09	25.15 ± 0.08	26.01 ± 0.17	25.83 ± 0.18

TABLE 5—*Continued*

MJD	Variables				
607.26	24.70 ± 0.11	25.14 ± 0.09	24.73 ± 0.08	25.82 ± 0.19	25.74 ± 0.13
609.67	24.72 ± 0.06	25.32 ± 0.08	25.13 ± 0.08	26.28 ± 0.13	...
609.68	24.69 ± 0.08	25.32 ± 0.10	...	25.82 ± 0.19	25.66 ± 0.13
612.55	24.81 ± 0.07	25.26 ± 0.09	25.05 ± 0.09	26.00 ± 0.13	25.72 ± 0.12
612.56	24.75 ± 0.06	25.18 ± 0.08	25.03 ± 0.11	25.83 ± 0.11	25.58 ± 0.13
615.50	24.81 ± 0.08	25.79 ± 0.14	25.22 ± 0.09	26.01 ± 0.16	25.32 ± 0.13
615.51	24.88 ± 0.11	25.85 ± 0.22	25.39 ± 0.12	26.48 ± 0.24	25.32 ± 0.10
619.39	...	...	25.74 ± 0.17	26.31 ± 0.12	24.89 ± 0.07
619.40	25.00 ± 0.07	26.01 ± 0.19	25.58 ± 0.13	26.00 ± 0.19	24.78 ± 0.11
623.61	25.10 ± 0.07	25.97 ± 0.16	25.54 ± 0.09	26.40 ± 0.15	25.03 ± 0.09
623.62	25.17 ± 0.10	25.60 ± 0.13	25.30 ± 0.06	26.50 ± 0.25	24.95 ± 0.08
629.31	25.39 ± 0.15	...	25.78 ± 0.22	25.39 ± 0.09	25.19 ± 0.10
629.32	25.34 ± 0.12	25.66 ± 0.14	25.75 ± 0.18	25.29 ± 0.11	25.13 ± 0.09
636.28	25.31 ± 0.15	24.81 ± 0.10	24.66 ± 0.08	25.51 ± 0.11	25.55 ± 0.08
636.29	25.25 ± 0.10	24.83 ± 0.08	...	25.70 ± 0.17	25.42 ± 0.09
643.25	24.75 ± 0.09	25.30 ± 0.10	25.05 ± 0.13	25.96 ± 0.14	25.62 ± 0.11
643.27	24.68 ± 0.07	25.29 ± 0.09	24.91 ± 0.07	25.98 ± 0.14	25.46 ± 0.17
653.57	25.07 ± 0.10	25.76 ± 0.14	...	26.60 ± 0.34	25.61 ± 0.12
653.59	...	25.73 ± 0.13	25.45 ± 0.12	26.13 ± 0.21	...
	C26	V01	V02	V03	
603.36	25.73 ± 0.09	24.87 ± 0.08	24.84 ± 0.05	25.49 ± 0.09	
603.38	...	24.86 ± 0.06	24.77 ± 0.11	25.41 ± 0.13	
605.30	25.51 ± 0.10	24.87 ± 0.05	24.70 ± 0.04	25.34 ± 0.11	
605.32	25.67 ± 0.10	24.87 ± 0.05	24.68 ± 0.07	25.38 ± 0.12	
607.25	...	...	24.50 ± 0.06	25.45 ± 0.13	
607.26	25.60 ± 0.14	24.86 ± 0.07	24.56 ± 0.07	25.40 ± 0.13	
609.67	25.48 ± 0.09	24.93 ± 0.10	24.58 ± 0.07	25.35 ± 0.11	
609.68	25.42 ± 0.09	24.89 ± 0.08	24.59 ± 0.07	25.39 ± 0.08	
612.55	24.80 ± 0.05	24.92 ± 0.05	24.51 ± 0.05	25.44 ± 0.09	
612.56	24.94 ± 0.05	...	24.58 ± 0.06	25.28 ± 0.10	
615.50	24.61 ± 0.08	24.98 ± 0.08	24.62 ± 0.06	25.40 ± 0.16	
615.51	24.71 ± 0.04	25.01 ± 0.10	24.55 ± 0.09	25.36 ± 0.10	
619.39	24.75 ± 0.04	24.85 ± 0.06	24.71 ± 0.10	...	
619.40	24.88 ± 0.05	24.92 ± 0.07	24.80 ± 0.10	25.15 ± 0.10	
623.61	25.00 ± 0.07	24.78 ± 0.05	24.84 ± 0.09	24.98 ± 0.10	
623.62	25.03 ± 0.06	24.82 ± 0.07	24.86 ± 0.12	...	
629.31	25.23 ± 0.12	24.69 ± 0.04	24.84 ± 0.06	24.83 ± 0.09	
629.32	25.07 ± 0.08	24.74 ± 0.10	...	24.87 ± 0.09	
636.28	25.48 ± 0.06	24.55 ± 0.06	25.06 ± 0.07	25.08 ± 0.07	
636.29	25.39 ± 0.07	24.44 ± 0.04	25.02 ± 0.08	24.98 ± 0.10	
643.25	25.70 ± 0.18	24.43 ± 0.05	25.23 ± 0.10	24.79 ± 0.17	
643.27	25.55 ± 0.05	24.34 ± 0.06	24.93 ± 0.08	25.21 ± 0.10	
653.57	24.86 ± 0.06	24.41 ± 0.09	25.36 ± 0.08	25.38 ± 0.11	
653.59	...	...	25.20 ± 0.06	25.32 ± 0.11	

Table 6
Individual I band photometric measurements

MJD	Variables				
	C01	C02	C03	C04	C05
603.42	25.91 ± 0.35	24.90 ± 0.19	24.97 ± 0.34	25.35 ± 0.23	23.88 ± 0.13
603.43	25.82 ± 0.27	24.73 ± 0.12	25.11 ± 0.31	25.39 ± 0.20	23.87 ± 0.14
609.73	25.54 ± 0.25	24.95 ± 0.31	25.14 ± 0.21	25.50 ± 0.26	23.86 ± 0.09
609.74	26.00 ± 0.60	25.04 ± 0.21	25.04 ± 0.19	25.51 ± 0.22	24.07 ± 0.14
619.45	26.16 ± 0.48	24.80 ± 0.46	24.84 ± 0.22	25.12 ± 0.17	24.35 ± 0.14
619.47	...	...	24.69 ± 0.16	25.00 ± 0.14	24.07 ± 0.16
629.37	25.54 ± 0.31	25.61 ± 0.43	25.31 ± 0.29	25.27 ± 0.16	23.96 ± 0.13
629.39	25.10 ± 0.14	25.52 ± 0.28	...	25.32 ± 0.30	24.16 ± 0.15
643.32	25.50 ± 0.24	25.13 ± 0.36	25.02 ± 0.16	25.09 ± 0.12	23.61 ± 0.09
643.33	25.38 ± 0.20	25.43 ± 0.34	25.44 ± 0.41	25.19 ± 0.21	23.75 ± 0.10
	C06	C07	C08	C09	C10
603.42	25.41 ± 0.24	24.59 ± 0.15	24.29 ± 0.38	25.34 ± 0.26	25.58 ± 0.26
603.43	25.09 ± 0.24	...	24.39 ± 0.16	24.89 ± 0.16	25.49 ± 0.37
609.73	24.59 ± 0.12	24.73 ± 0.28	24.22 ± 0.15	24.95 ± 0.18	25.13 ± 0.31
609.74	24.69 ± 0.17	24.45 ± 0.12	24.35 ± 0.12	24.78 ± 0.08	24.97 ± 0.19
619.45	25.08 ± 0.21	25.21 ± 0.36	24.50 ± 0.22	24.75 ± 0.15	25.23 ± 0.25
619.47	25.22 ± 0.34	24.66 ± 0.15	24.64 ± 0.19	24.77 ± 0.14	25.13 ± 0.28
629.37	24.57 ± 0.09	24.32 ± 0.14	24.28 ± 0.11	24.94 ± 1.04	24.85 ± 0.18
629.39	24.64 ± 0.15	24.83 ± 0.15	24.56 ± 0.24	25.57 ± 0.49	24.99 ± 0.22
643.32	25.42 ± 0.23	24.55 ± 0.12	24.23 ± 0.14	25.05 ± 0.19	25.23 ± 0.21
643.33	25.32 ± 0.23	24.06 ± 0.47	24.23 ± 0.16	24.59 ± 0.09	...
	C11	C12	C13	C14	C15
603.42	...	24.99 ± 0.15	25.13 ± 0.20	24.87 ± 0.18	25.52 ± 0.28
603.43	...	24.91 ± 0.15	25.23 ± 0.22	25.03 ± 0.13	25.50 ± 0.40
609.73	25.12 ± 0.37	...	25.05 ± 0.18	25.30 ± 0.20	24.64 ± 0.15
609.74	24.81 ± 0.23	24.80 ± 0.19	25.54 ± 0.24	25.12 ± 0.18	24.78 ± 0.16
619.45	...	25.00 ± 0.16	...	...	24.90 ± 0.18
619.47	...	24.83 ± 0.12	...	...	25.55 ± 0.28
629.37	24.57 ± 0.19	24.60 ± 0.11	25.26 ± 0.24	...	24.43 ± 0.10
629.39	24.72 ± 0.12	24.72 ± 0.14	...	25.27 ± 0.18	24.70 ± 0.12
643.32	24.73 ± 0.27	25.02 ± 0.30	...	25.80 ± 0.35	25.54 ± 0.25
643.33	25.21 ± 0.25	24.83 ± 0.13	...	...	25.18 ± 0.21
	C16	C17	C18	C19	C20
603.42	25.25 ± 0.48	25.21 ± 0.24	24.87 ± 0.21	24.78 ± 0.10	24.56 ± 0.15
603.43	25.34 ± 0.31	25.13 ± 0.27	24.58 ± 0.13	24.66 ± 0.15	24.67 ± 0.16
609.73	25.54 ± 0.39	25.44 ± 0.21	25.17 ± 0.41	24.68 ± 0.24	25.26 ± 0.16
609.74	25.27 ± 0.43	25.33 ± 0.33	24.98 ± 0.18	24.58 ± 0.17	25.23 ± 0.13
619.45	24.95 ± 0.21	24.67 ± 0.12	24.70 ± 0.15	25.13 ± 0.33	25.15 ± 0.21
619.47	24.72 ± 0.17	24.99 ± 0.28	24.28 ± 0.10	25.52 ± 0.29	...
629.37	...	25.02 ± 0.21	24.84 ± 0.16	24.52 ± 0.14	24.72 ± 0.20
629.39	24.99 ± 0.19	24.76 ± 0.17	24.67 ± 0.10	24.80 ± 0.14	24.60 ± 0.10
643.32	24.60 ± 0.19	25.05 ± 0.34	24.79 ± 0.21	24.93 ± 0.14	...
643.33	24.53 ± 0.17	24.76 ± 0.22	24.78 ± 0.16	25.11 ± 0.26	25.09 ± 0.17
	C21	C22	C23	C24	C25
603.42	...	24.05 ± 0.10	24.08 ± 0.10	24.47 ± 0.14	...
603.43	24.18 ± 0.10	23.94 ± 0.12	24.10 ± 0.10	24.55 ± 0.20	24.54 ± 0.17
609.73	23.72 ± 0.07	24.05 ± 0.08	24.20 ± 0.21	24.57 ± 0.12	24.66 ± 0.16
609.74	23.75 ± 0.06	24.11 ± 0.12	24.26 ± 0.10	24.73 ± 0.21	24.59 ± 0.12
619.45	24.00 ± 0.11	24.34 ± 0.11	24.59 ± 0.17	24.87 ± 0.20	24.02 ± 0.07
619.47	24.07 ± 0.09	24.29 ± 0.11	24.59 ± 0.19	25.04 ± 0.21	23.99 ± 0.10
629.37	24.19 ± 0.11	24.48 ± 0.15	24.64 ± 0.19	24.68 ± 0.14	24.12 ± 0.10
629.39	24.34 ± 0.18	24.56 ± 0.14	24.72 ± 0.15	24.37 ± 0.11	23.98 ± 0.08

TABLE 6—*Continued*

MJD	Variables				
643.32	23.91 ± 0.07	...	23.97 ± 0.07	24.78 ± 0.14	24.77 ± 0.20
643.33	23.87 ± 0.09	24.01 ± 0.08	24.15 ± 0.14	24.60 ± 0.14	24.66 ± 0.18
	C26	V01	V02	V03	
603.42	24.50 ± 0.16	23.60 ± 0.06	23.43 ± 0.06	24.19 ± 0.14	
603.43	24.78 ± 0.21	23.73 ± 0.09	23.49 ± 0.04	24.03 ± 0.09	
609.73	24.12 ± 0.08	23.75 ± 0.27	23.29 ± 0.23	24.14 ± 0.13	
609.74	24.35 ± 0.18	23.77 ± 0.05	23.42 ± 0.08	24.03 ± 0.13	
619.45	23.89 ± 0.09	23.72 ± 0.06	23.37 ± 0.04	24.16 ± 0.09	
619.47	23.88 ± 0.10	23.70 ± 0.09	23.48 ± 0.06	24.15 ± 0.11	
629.37	24.01 ± 0.10	23.56 ± 0.06	23.53 ± 0.07	23.77 ± 0.09	
629.39	23.92 ± 0.09	23.48 ± 0.06	23.58 ± 0.08	23.83 ± 0.08	
643.32	24.26 ± 0.11	23.49 ± 0.04	23.69 ± 0.07	...	
643.33	24.43 ± 0.11	23.44 ± 0.09	23.65 ± 0.06	23.84 ± 0.09	

TABLE 7
ERROR BUDGET FOR THE CEPHEID DISTANCE TO NGC 2841

Item	Value (mag)
Dispersion in μ_0	± 0.06
Metallicity correction	± 0.15
LMC distance	± 0.10
WFPC2 calibration	± 0.07
Blending	$+0.10$
Total	$+0.23, -0.20$

TABLE 8
GALAXIES WITH CEPHEID DISTANCES IN THE LEO CLOUD & SPUR

Name	Cepheid distance (Mpc)	R.A. (J2000.0)	Dec. (J2000.0)	cz km/s	Super-galactic coordinates Long. (°)	Lat. (°)	X (Mpc)	Y (Mpc)	Z (Mpc)
NGC 2541	11.2	08:14:40.2	+49:03:42	559 ± 1	40.5	-22.9	7.8	6.7	-4.4
NGC 2841	14.1	09:22:02.7	+50:58:36	638 ± 3	49.6	-16.0	8.7	10.3	-3.9
NGC 3198	13.8	10:19:54.9	+45:32:59	663 ± 4	60.6	-13.3	6.6	11.7	-3.2
NGC 3319	13.3	10:39:08.8	+41:41:16	739 ± 1	66.0	-12.8	5.3	11.8	-2.9
NGC 3351	10.0	10:43:57.8	+11:42:14	778 ± 4	94.1	-27.1	-0.6	8.9	-4.6
NGC 3368	10.5	10:46:45.7	+11:49:12	897 ± 4	94.3	-26.4	-0.7	9.4	-4.7
NGC 3621	6.6	11:18:16.0	−32:48:42	727 ± 5	145.7	-28.5	-4.8	3.3	-3.2
NGC 3627	10.1	11:20;15.0	+12:59:30	727 ± 3	96.6	-18.4	-1.1	9.5	-3.2